Vol. 48 No. 1 Journal of the Communications Research Laboratory March 2001
Printed in Tokyo, Japan pp. 173–195

4.8 Exploration of Solar Wind Acceleration Region Using Interplanetary Scintillation of Water Vapor Maser Source and Quasars

By
Munetoshi TOKUMARU, Yohei YAMAUCHI, and Tetsuro KONDO

ABSTRACT

Single-station observations of interplanetary scintillation (IPS) at three microwave frequencies; 2 GHz, 8 GHz and 22 GHz have been carried out between 1989 and 1998 using a large (34 mϕ) radio telescope at the Kashima Space Research Center of the Communications Research Laboratory. The aim of these observations is to explore the near-sun solar wind, which is the key region for the study of the solar wind acceleration mechanism. Strong quasars; 3C279 and 3C273B were used for Kashima IPS observations at 2 GHz and 8 GHz, and a water vapor maser source, IRC20431 was used for the IPS observations at 22 GHz. Solar wind velocities derived from Kashima IPS data suggest that the solar wind acceleration takes place at radial distances between 10 and 30 solar radii (R_S) from the sun. Properties of the turbulence spectrum (e.g. anisotropy, spectral index, inner scale) inferred from Kashima data are found to change systematically in the solar wind acceleration region. While the solar wind in the maximum phase appears to be dominated by the slow wind, fast and rarefied winds associated with coronal holes are found to develop significantly at high latitudes as the solar activity declines. Nevertheless, Kashima data suggests that the location of the acceleration region is stable throughout the solar cycle.

Keywords: Solar wind, Interplanetary scintillation, Space plasma physics

1. Introduction

The existence of the solar wind—a plasma stream flowing out from the sun at supersonic speed—was first predicted theoretically by Parker[1], and was subsequently confirmed by direct measurements using spacecraft in the early 1960s[2]. The discovery of the solar wind is of great importance because it has revealed the existence of way in which the terrestrial environment (especially the electromagnetic environment) is connected to the sun. That is, it became clear that the sun and earth form a closely-coupled system via the medium of the solar wind, and that disturbances in the Earth's magnetosphere originate from solar activity. Research on the solar-terrestrial system was originally conducted from a purely scientific viewpoint, but in recent years as our lives depend increasingly on information services provided from space (broadcasting, communication, remote sensing, etc.), it has become impossible to ignore the effects of solar activity on these services, and research on the solar-terrestrial system has been the focus of growing interest from a viewpoint of applications. Solar activity causes a serious effect in many fields, including the failure of satellite equipment, the exposure of astronauts to radioactivity, the interruption of radio communications, and power surges in transmission lines and submarine cables. In the future, as our society becomes increasingly dependent on information technology, it can be concluded that "space weather forecast" services for predicting the effects of solar activity before they happen will become indispensable. Based on this view, various space weather forecasting research projects are underway at many establishments, including NASA in the US. The Communications Research Laboratory (CRL) is playing a crucial role in this research, and it is noteworthy that the CRL initiated the "space weather forecast" project[3] in 1988, leading other space weather researches.

Since the solar wind was discovered, the physical processes arising in the solar-terrestrial system have been clarified from a wide variety of studies, and a number of these phenomena have been reproduced in computer simulations. But even with the best knowledge currently available, it is still difficult to predict the occurrence of space environment disturbances in the vicinity of the earth from solar observation data. One reason for this is that we still do not precisely understand where or how the solar wind is generated. Although the Parker's model demonstrates the existence of the solar wind, there are many properties of the actual solar wind that this model is unable to explain. Various improved solar wind models have been proposed[4], but none of these can describe the behavior of the actual solar wind completely. The shortfalls in our understanding of the formation (acceleration) of the solar wind arise entirely from the lack of observation data in the regions where the solar wind is generated. From earlier studies, the solar wind is considered to form in a region covering the radial distance range between several solar radii (R_S) and several tens of solar radii from the sun (see Fig. 1[5]). This region has never been probed directly by spacecraft, so we still have to rely on investigations by remote-sensing measurement. Since intense radiations from the vicinity of the solar surface are observed over a wide range of frequencies, it is possible to perform detailed investigation of the

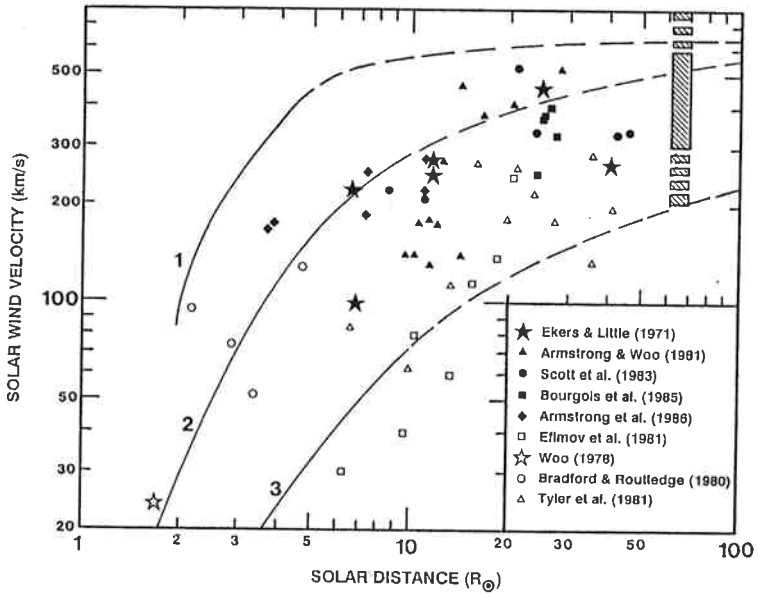

Fig. 1 **The radial dependence of the solar wind velocities obtained from various kinds of earlier microwave IPS observations (after Bird et al.[5]). The vertical line at 62 $R_\odot$ indicates the range of solar wind velocities measured by the Helios spacecraft at its closest approach to the sun. The solid lines of (1), (2), and (3) represent the radial variation of solar wind speed obtained from coronagraph observations, a solar wind model including the pressure exerted by MHD wave, and a solar wind model without the MHD wave pressure, respectively.**

characteristics and behavior of the solar atmosphere from remote-sensing observations of these radiations. But since the density of the solar wind formation region (from several R_S to several tens of R_S) is extremely low, it is impossible to observe the radiation from the plasma itself. This makes it difficult to perform observational studies in this region.

The only feasible way of investigating the solar wind acceleration region is to observe it using interplanetary scintillation (IPS) in the microwave frequency band[6,7,8]. IPS is the phenomenon caused by the scattering of radio waves by density fluctuations in the plasma; intensity variation, which is the diffraction pattern due to the mutual interference of radio waves, are observed on the earth[9,10]. IPS is observed for radio waves from compact radio sources with a small apparent size, so quasars and masers are often used for this purpose. The solar wind region that can be studied by IPS depends on the observation frequency, and in order to probe the solar wind closer to the sun, it is necessary to observe IPS at higher frequencies. IPS at microwave frequencies (of the order of GHz) is sensitive to the solar wind over the range from several R_S to several tens of R_S, which is suitable for observing the acceleration region.

Although a number of attempts have already been made to observe the solar wind acceleration region using microwave IPS, they have produced little data, and the solar wind acceleration mechanism has never understood yet. The scarcity of IPS data in the microwave band arises from the lack of radio sources and facilities (antennas) that can be used for observations. Less flux is emitted by celestial radio sources at higher frequencies, but since IPS is a phenomenon varying over time scales ranging from a few seconds down to a tenth of a second, it is impossible to improve the S/N ratio by using long-time integration. It is thus inevitable that the observations are restricted to strong radio sources, even when the large antenna is used. In addition, there are severe limitations on the time available for their use, since most of antennas large enough for IPS observation are shared facilities.

Between 1989 and 1998, the large (34 m aperture) radio telescope at the Kashima Space Research Center of CRL was used to clarify the solar wind generation (acceleration) mechanism, and IPS observations were made at three microwave frequencies (2 GHz, 8 GHz and 22 GHz)[11-17]. In this report, we provide an overview of the Kashima IPS observations and discuss the main achievements made as a result. It is unprecedented for such a large antenna to be used for microwave IPS observations over almost an entire 11-year solar cycle. Furthermore, 22 GHz is the highest observation frequency ever used for IPS observations, and allows us to probe the solar wind up to a distance of just $5R_S$ from the sun. These characteristics mean that the Kashima IPS data is of great importance for study of solar wind acceleration. Furthermore, the period over which the observations were made covers the international Solar-Terrestrial Energy Program (STEP), and a variety of observations were made all over the world as part of this campaign. Our IPS observations constituted one part of this effort[18-23]. During this period, two important developments were made in the study of the solar wind acceleration mechanism. First, observations made by the *Ulysses* high-latitude

solar wind spacecraft led to the establishment of the two-component (fast and slow winds) solar wind model[24], and second, the rapid acceleration of the fast wind was discovered by long-baseline IPS observations at microwave frequencies[25]. The fact that the Kashima IPS observations were made during this important period is very meaningful.

2. Observations

Table 1 lists the radio sources used in the Kashima IPS observations. The radio sources used here (quasars and H_2O masers) are compact, but have a relatively strong electromagnetic flux, and the apparent positions get close to the sun (within 30 R_S). Among the quasars listed in the table, valid data were obtained from IPS observations for 3C273B and 3C279, and the data from the other stars had a low S/N ratio and was not used in this analysis. The observations were made at frequencies of 2 GHz and 8 GHz for quasars (Simultaneous observations at 2 GHz and 8GHz have performed since 1990), and 22 GHz for H_2O maser radio sources.

The Kashima IPS observations were made every year from 1989 to 1998 except for 1996; the quasar observations were made from late September to early October, and the H_2O maser observations were made in late December. Table 2 summarizes the conditions of the Kashima IPS observations. Faults in the Kashima 34 m antenna made it unavailable for use in 1992 and 1993, so

Table 1 The radio sources used in the Kashima IPS observations

Name	Type	R.A. (B1950)	Dec. (B1950)	Closest approach to the sun	
				Date	Distance (RS)
1148-001	QSO	11h 48' 11"	−00d 07' 32"	Sep. 20	22
3C273B	QSO	12h 26' 33"	+02d 19' 43"	Sep. 28	18
3C279	QSO	12h 53' 36"	−05d 31' 08"	Oct. 08	<1
1306-09	QSO	13h 06' 01"	−09d 34' 28"	Oct. 13	9
IRC20431	WVM	18h 05' 03"	−22d 13' 56"	Dec. 23	5

QSO: Quasar, WVM: Water Vapor (H_2O) Maser

Table 2 Summary of Kashima IPS observations

Observation year	Period	Radio source	Remarks
1989	Sep. 22 - Oct. 16	3C273B, 3C279	
1989	Dec. 21 - Dec. 26	IRC20431	
1990	Sep. 20 - Oct. 19	3C273B, 3C279	The first use of the dedicated back-end system
1990	Dec. 21 - Dec. 26	IRC20431	
1991	Sep. 20 - Oct. 20	3C273B, 3C279	Receiver bandwidth changed, and the automatic gain control available
1991	Dec. 20 - Dec. 27	IRC20431	
1992	Sep. 22 - Oct. 12	3C273B, 3C279	Observation made using GSI's 26 m antenna, Sampling period changed
1993	Sep. 21 - Oct. 20	3C273B, 3C279	Observation made using GSI's 26 m antenna, Number of continuous samples increased
1994	Sep. 19 - Oct. 17	3C273B, 3C279 1148-001, 1306-09	
1994	Dec. 21 - Dec. 27	IRC20431	Observations made at the room temperature after Dec. 23 due to a receiver fault
1995	Oct. 3 - Oct. 20	3C273B, 3C279 1306-09	
1997	Oct. 8 - Oct. 19	3C273B, 3C279	
1997	Dec. 22 - Dec. 28	IRC20431	Unable to receive radio source
1998	Sep. 19 - Oct. 19	3C273B, 3C279 1148-001	

the observations were carried out using the Kashima 26 m antenna belonging to the Geographical Survey Institute. The Kashima 26 m antenna is unable to receive at 22 GHz, so no H_2O maser observations were made during this period. Also, from 1995 onwards, it became impossible for the 34 m antenna to receive the H_2O maser source IRC20431 that had been used for the observations, so no 22 GHz IPS observations were made after 1995. Although it is not clear why this source could no longer be received, possible causes are a drop in the intensity of the H_2O maser source or a drop in the receiver efficiency of the 34 m antenna at 22 GHz. During the period shown in Figure 2, the IPS observations were performed continuously each day between 8 hr JST and 16 hr JST. However, since maintenance/repair work and other experiments such as VLBI were given higher priority even during this period, the IPS observations were sometimes interrupted.

In the Kashima IPS observations, the IPS data was collected using the IF signal outputs from an existing front-end unit (for a description of the 34 m antenna receiver system, see Koyama et al.[26]). During the initial observation period in 1989, the IF output was connected to a spectral analyzer, and the detected outputs from this analyzer were sampled by the PC dedicated for the IPS observations. In the quasar observations made from 1990 onwards, the data was collected using the newly-developed back-end system for the IPS observations. This IPS back-end system has two channels for use at 2 GHz and 8 GHz, each channel consisting of a programmable attenuator for gain control (added in 1991), a band-pass filter, an amplifier, a detector, and a low-pass filter with a cut-off frequency of 25 Hz. The bandwidth of the band-pass filter was either 80 MHz (1990) or 40 MHz (from 1991 onwards) for 2 GHz signals, and 190 MHz (1990) or 120 MHz (from 1991 onwards) for 8 GHz signals. The H_2O maser observations were made using a spectral analyzer and the data acquisition PC in the same way as in 1989.

The IPS data acquisition PC allows us to sample two channels of IPS data simultaneously (except in 1989 when only one channel was available), and to collect data automatically at programmed times. This data acquisition PC is also capable of controlling the programmable attenuator of the back-end system. Sampled signals are obtained as 12-bit data with a sampling period of 20 milliseconds (up to 1991) or 12 milliseconds (from 1992 onwards). A total of 30,000 (up to 1993) or 41,000 (from 1994 onwards) samples can be acquired continuously. The acquired data was stored on magneto-optical disks for subsequent analysis on a workstation.

Figure 2 shows the intensity data obtained from the observations for the quasar 3C273B with the Kashima 34 m antenna. These observations were made at 2 GHz (S band) and 8 GHz (X band). In this figure, the antenna was repeatedly directed towards (on-source) and away from (off-source) the radio source at intervals of approximately one minute. The IPS appears as very strong variations in the on-source data. In the actual observations, the on-source and off-source observations for a

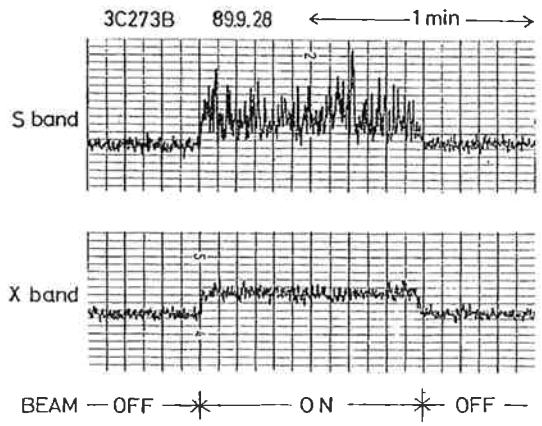

Fig. 2 The intensity variation of 3C273B observed with the Kashima 34 m antenna. The upper panel corresponds to 2 GHz (S band) data, and the lower panel corresponds to 8 GHz (X band) data. When the antenna beam is directed to the radio source (on-source), the received level increases and the intensity fluctuates due to IPS.

given radio source were repeated at 15-minute intervals, and data was acquired from each of these. In the off-source observations, the beam was shifted to either the eastward or the westward, whichever was further away from the sun with respect to the radio source. The off-source displacement was 30 minutes for quasars and 5 minutes for H_2O masers. The off-source data was used to evaluate the intensity fluctuations arising from background components.

3. Analysis

To estimate the solar wind velocity from IPS observations, the cross-correlation method is usually employed; that is, a time difference is determined by cross-correlation processing from IPS data obtained at multiple stations, and this time difference is converted into a speed[27,28]. However, a single station was used for the Kashima IPS experiments, so it is impossible to use the cross-correlation method. Instead, in the Kashima IPS experiments, the solar wind velocity was estimated using a spectral fitting method[29] and a cospectrum method[30]. The spectral fitting method has an advantage that it allow us to determine not only the solar wind velocity, but also information on the spatial spectrum of solar wind density fluctuations. We also determined the scintillation index[29] from the obtained IPS data, and analyzed the distribution of the solar wind density fluctuations. An explanation of these analysis methods is presented below.

3.1 Spectral fitting method

When radio waves are scattered weakly ($\Delta\phi^2 < 1$ rad.) by density fluctuations in the solar wind plasma, and when multiple scattering effects are ignored (the Born approximation is valid), the IPS power spectrum $P(f)$ is expressed as follows[31]:

$$P(f) = \int_0^\infty P'(f,z)\,dz \quad \cdots\cdots(1)$$

$$P'(f,z)dz = 2\pi\lambda r_e \int_0^\infty \frac{p(V_\perp)}{|V_\perp|} dV_\perp \int_{-\infty}^{\infty} \Phi_{ne}\left(k_x = \frac{2\pi f}{V_\perp}, k_y, z\right) \times F_{diff}(k_x, k_y, k_z) F_{source}(\vec{k}) F_{receiver}(\vec{k})\,dk_y dz, \quad \cdots\cdots(2)$$

where $\vec{k} = (k_x, k_y, k_z = 0)$ is the spatial wave vector, z is the distance along the line-of-sight, λ is the observation wavelength, r_e is the classical electron radius ($=2.8\times10^{-13}$ cm), $V_\perp$ is the solar wind velocity projected onto a plane perpendicular to the line of sight, and $p(v)$ is the solar wind velocity distribution function (for components parallel to the flow direction). The frequency f of intensity variation due to IPS is given by $f = V_\perp k_x/2\pi$. Model calculations show that the shape of the power spectrum is insensitive to $p(v)$. Accordingly, in the following analysis by spectral fitting, velocity fluctuations in the solar wind are ignored and a uniform flow is assumed; $p(v) = \delta(v = V_\perp)$.

In Equation (2), F_{diff} is the Fresnel filter term, which is expressed as follows.

$$F_{diff} = 4\sin^2\left(\frac{k^2\lambda z}{4\pi}\right) \quad \cdots\cdots(3)$$

This term has the property of cutting off spatial wave numbers less than $k_F = (4\pi/\lambda z)^{1/2}$. F_{source} and $F_{reciever}$ correspond to the effect of the apparent size of the radio source and that of the receiver bandwidth respectively, and those are expressed as follows.

$$F_{source}(\vec{k}) = \exp(-k^2/k_s^2) \quad \cdots\cdots(4)$$

$$F_{reciever}(\vec{k}) = \exp(-k^2/k_r^2) \quad \cdots\cdots(5)$$

where $k_s = 1/z\theta_0$, $k_r = k_F(\Delta\lambda/\lambda)^{1/2}$, and θ_0 and $\Delta\lambda$ are the apparent angular size of the radio source and the bandwidth (wavelength) of the receiver, respectively. As these equations show, F_{source} and $F_{reciever}$ have the property of cutting off components with large spatial frequencies.

Φ_{ne} is the spatial spectrum of solar wind (electron) density fluctuations, and it is known from previous observations[32] that Φ_{ne} is well expressed by the following equation.

$$\Phi_{ne}(\vec{k}) = \Delta N_e^2 (k_x^2 + (k_y/AR)^2)^{-\alpha/2} \exp(-k^2/k_i^2) \quad \cdots\cdots(6)$$

where ΔN_e is solar wind (electron) density fluctuations, α is the power-law index of the spatial spectrum, AR is the axial ratio of anisotropy of density fluctuations, and k_i is the spatial wave number corresponding to the inner scale of the density fluctuations. The effect of the inner scale is the same as the effect of the apparent size of the radio source and the effect of the receiver bandwidth, and it acts as a filter that cuts off high frequency wave numbers. Consequently, these three effects are represented using an equivalent cut-off wave number k_{eq} as given by the following equation.

$$1/k_{eq}^2 = 1/k_s^2 + 1/k_r^2 + 1/k_i^2 \quad \cdots\cdots(7)$$

As the above equations show, the IPS power spectrum $P(f)$ is closely related to the solar wind velocity and the spatial spectrum of density fluctuations. It is thus possible to estimate the solar wind velocity and the spatial spectrum of density fluctuations by optimizing the spectrum $P(f)$ calculated from Equations (1) and (2) to the observed spectrum. This is a basic idea for the spectral fitting method[29]. In Equations (1) and (2), although the scattering by the solar wind is assumed to be weak, the density fluctuations become larger as getting closer to the sun, and the radio wave scattering also increases, until this weak scattering assumption no longer holds. This imposes a limit on the applicability of the spectral fitting method. Earlier studies have shown that the distance of the applicable limit is about 10 R_S at 2 GHz, about 4 R_S at 8 GHz, and about 1.7 R_S at 22 GHz. Since most of radio sources do not approach to this distance limit, the distance of closest approach of the radio source gives the minimum observable distance in IPS observations.

As Equation (1) shows, $P(f)$ is an integral along the line of sight, so that knowledge of the three-dimensional structure of the solar wind is needed to perform the model calculations. If a large number of radio sources are used for IPS observations, the three-dimensional structure of the solar wind can be inferred by applying computer tomography techniques, which enable us to determine the three-dimensional structure by optimizing the model to the observations[33]. However, in the Kashima IPS experiment only a few sources were observed in a day, making it impossible to apply computer tomography techniques. Therefore, in the Kashima IPS experiment, the data is analyzed based on the assumption that the contribution to the IPS observed on the ground mostly comes from the point closest to the sun on the line of sight (so-called point P; see Fig. 3, this assumption is called the "point P" approximation). Equation (6) shows that the magnitude of Φ_{ne} is proportional to solar wind density fluctuations ΔN_e^2 and solar wind density fluctuations are assumed to distribute isotropically, i.e. $\Delta N_e^2 \propto R^{-2}$ (where R is distance from the sun), thus the magnitude of $P(f,z)$ is considered to be proportional to R^{-4}. This means that the greatest contribution to the integral of IPS along the line of sight comes from the point-P. Using the point P approximation, $P(f)$ is given as follows.

$$P(f) = P'(f, z = Z) \quad \cdots\cdots(8)$$

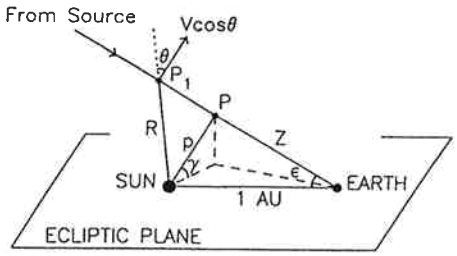

Fig. 3 The geometrical relationship of the line of sight for IPS observations.

where Z is the distance from point P to the earth. At point P, the plane perpendicular to the line of sight coincides with the radial direction, and the solar wind is considered to flow approximately along the radial direction beyond the flow source plane (2.5 R_S), so that $V_\perp$ is considered to match the true speed V of the solar wind under the point P approximation. Figure 4 shows an example of an IPS power spectrum calculated using the above equation with parameters optimized for an observed spectrum (from IPS observations for the H_2O maser source IRC203431 in 1989). Here, the solar wind velocity was taken as a free parameter; the other parameters were fixed. As this figure shows, the observed power spectrum closely matches the model calculations, and from this analysis the solar wind velocity is inferred to be 33 km/s (for the point P at a distance of 5 R_S).

3.2 Cospectrum method

In principle, the spectral fitting method allows us to determine many solar wind parameters (including the solar wind velocity) simultaneously from IPS data obtained from single-station measurements at a given frequency. However, the reliability of solar wind parameters obtained from the spectral fitting analysis is limited by the effect of noise inherent to actual IPS data, and an extremely excellent S/N ratio (e.g. $\geq$ 30 dB) would be required to obtain reliable estimation for multiple parameters from the spectral fitting analysis. It is also difficult to distinguish effects of different solar wind parameters, such as the solar wind velocity and the axial ratio of density fluctuations, in the observed power spectrum. In particular, when the density fluctuations are highly anisotropic, reliable velocity estimates are hardly obtained from the spectrum fitting analysis. Instead, we have employed here a cospectrum method, by which the solar wind velocity is derived from IPS data obtained simultaneously at two frequencies (2 GHz and 8 GHz). The

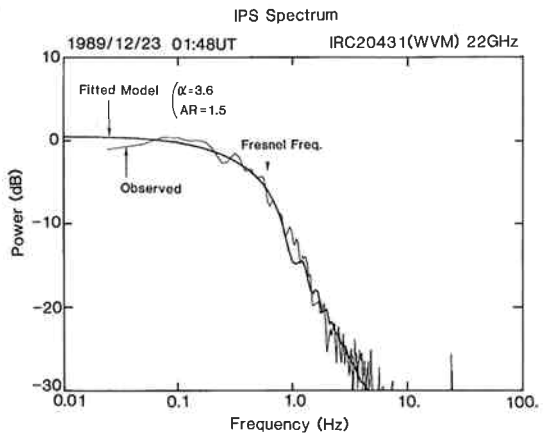

Fig. 4 An example of the IPS power spectrum observed at 22 GHz with the Kashima 34 m antenna[11]. This observation was obtained in 1989 for the H_2O maser source of IRC20431. The heavy line shows the model calculations of the IPS power spectrum with parameters optimized for the observations.

cospectrum method was first proposed by Scott et al.[30], who demonstrated from simultaneous IPS observations at three UHF frequencies that this method acts as a reliable measurement of the solar wind speed. The cospectrum method has the advantage of allowing us to determine the solar wind velocity without a bias due to the anisotropy of the solar wind, even using IPS data with a relatively low S/N ratio, while no application of the cospectrum method had been made before our study.

In the cospectrum method, a normalized cospectrum $NCS(f)$ is calculated from IPS data at two frequencies using the following equation.

$$NCS(f) = \frac{R_e(S_{12}(f))}{\sqrt{P_1(f)\cdot P_2(f)}} \quad \cdots\cdots (9)$$

where $R_e(S_{12}(f))$ is the real part of the correlation spectrum $S_{12}(f)$ between two frequencies, and $P_1(f)$ and $P_2(f)$ correspond to the power spectra at two frequencies respectively. Using the weak scattering assumption, the Born approximation (where the effect of multiple scattering is neglected) and the point P approximation (where contributions at $z = Z$ to IPS are considered; see the previous section), we can write $S_{12}(f)$ as follows:

$$S_{12}(f) = \pi r_e^2 \lambda_1 \lambda_2 \int_0^\infty \frac{2\pi}{V_\perp} p(v)\,dv \int_{-\infty}^{\infty} \Phi_{ne}(\vec{k}) \sin\left(\frac{k^2\lambda_1 Z}{4\pi}\right) \sin\left(\frac{k^2\lambda_2 Z}{4\pi}\right) \times F_{source}(\vec{k}) F_{receiver}(\vec{k})\,dk_y \quad \cdots\cdots (10)$$

where λ_1 and λ_2 represent the wavelengths corresponding to the two frequencies. Figure 5 displays the normalized cospectrum $NCS(f)$ calculated from Equation (10) and a normalized cospectrum $NCS(f)$ obtained from the Kashima IPS observations. As demonstrated in this figure, the observed spectrum show an excellent agreement with the calculated one. $NCS(f)$ has a positive value at low frequencies, while at higher frequencies it shows a sinusoidal variation. Here, the frequency at which it first crosses zero, f_{ZERO}, is related to the solar wind velocity V through the following equation:

$$V = K f_{ZERO} \sqrt{\lambda_1 Z} \quad \cdots\cdots (11)$$

where λ_1 is the wavelength corresponding to the lower observation frequency (2 GHz in this study) and K is a correction coefficient. In the Kashima IPS observations, the distance range for which Equation (11) is applicable is given by the weak scattering assumption for 2 GHz, which holds for distances up to about 10 R_S from the sun. Any IPS data taken within this limit were not used for the current analysis.

It is noteworthy that the correction coefficient K hardly changes even when solar wind parameters such as the density anisotropy and the spatial spectral index vary greatly. Table 3 shows how the correction coefficient K changes with various solar wind parameters. Even when AR, α and k_{eq}/k_F are changed, K is found to remain within the range 1.1-1.2. The only exception is when the random velocity δv (the velocity component parallel to the flow) increases: as the table shows, K increases with

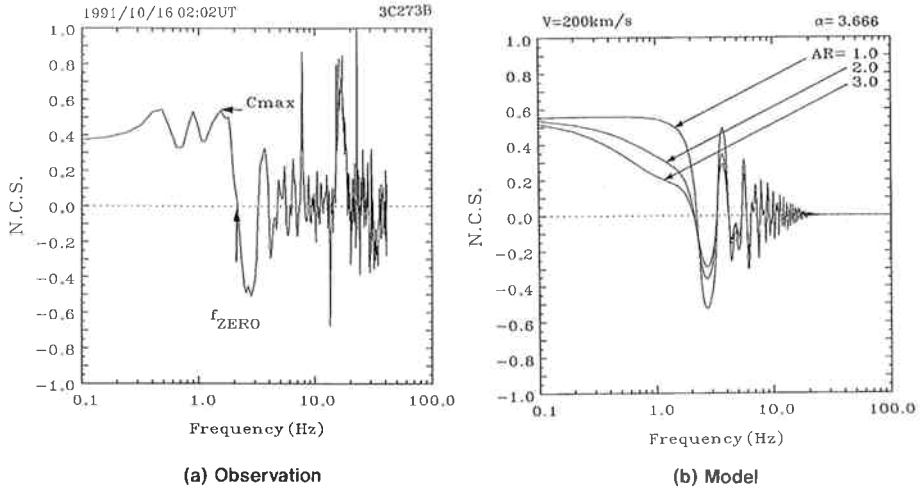

Fig. 5 (a) **An example of the normalized cospectrum** $NCS(f)$ **obtained from Kashima IPS observations.** (b) **The model calculations of** $NCS(f)$ **with axial ratios of** $AR=1.0$, **2.0 and 3.0. The observation frequencies are 2 GHz and 8 GHz.**

Table 3 The value of K **for various solar wind parameters (obtained using the point P approximation).**

Axial ratio AR	Spectral index α	Equivalent cut-off wave number keq/kF	Random velocity $\delta v/V$	K
1.0	3.6	100	0.0	1.12
1.5	3.6	100	0.0	1.15
2.0	3.6	100	0.0	1.17
3.0	3.6	100	0.0	1.19
5.0	3.6	100	0.0	1.20
10.0	3.6	100	0.0	1.21
1.0	2.0	100	0.0	1.15
1.0	3.0	100	0.0	1.13
1.0	4.0	100	0.0	1.11
1.0	3.6	20	0.0	1.12
1.0	3.6	10	0.0	1.12
1.0	3.6	5	0.0	1.12
1.0	3.6	100	0.1	1.12
1.0	3.6	100	0.3	1.07
1.0	3.6	100	0.4	1.00
1.0	3.6	100	0.5	0.93
1.0	3.6	100	0.8	0.74

increasing δv. Here, a Gaussian distribution is assumed for $p(v)$. This means the velocity V_{ZERO} determined from Equation (11) with a constant value for K differs greatly from the true solar wind velocity V when a large random velocity exists. Figure 6 shows how this difference depends on the random velocity when a constant value of $K=1$ is used. As far as the random velocity does not exceed about 30% of the solar wind velocity, V_{ZERO} is about 10% lower than the true velocity V, but V_{ZERO} becomes greater than the true velocity as the random velocity increases, and when the random velocity is about 90%, V_{ZERO} becomes as high as 1.5 times the true velocity.

In this study, we determined the solar wind velocity from Equation (11) assuming that the effects of random velocity are small, and we used either $K=1$ or $K=1.25$. For example, the table shows that the velocity V_{ZERO} determined from Equation (11) with $K=1$ lies within (10% of the true velocity V as far as the random velocity is within about 50% of the solar wind velocity. Here, it should be noted that this calculation ignores the effects of line-of-sight integration, only considering the contribution at point P (point P approximation). The line-of-sight integration has the effect to yield a lower velocity estimate than the true solar wind speed when $K=1$ is used, and we have confirmed from model calculations (see section 4.1) that a value of $K=1.25$ is more suitable for

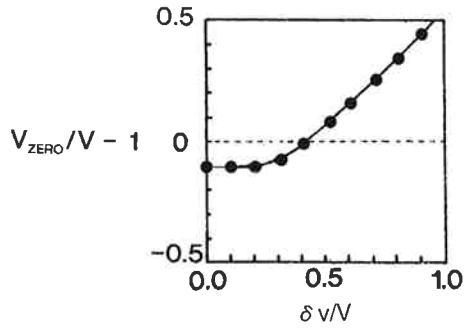

Fig. 6 The difference between the solar wind velocity derived with the cospectrum method and the true velocity of the solar wind, plotted as a function of a ratio $\delta v/V$, where δv and V are the random velocity (parallel to the flow direction) and the bulk flow speed of the solar wind, respectively. Here, it is assumed that $K=1$, and the vertical axis shows the ratio of the velocity difference with respect to the true value.

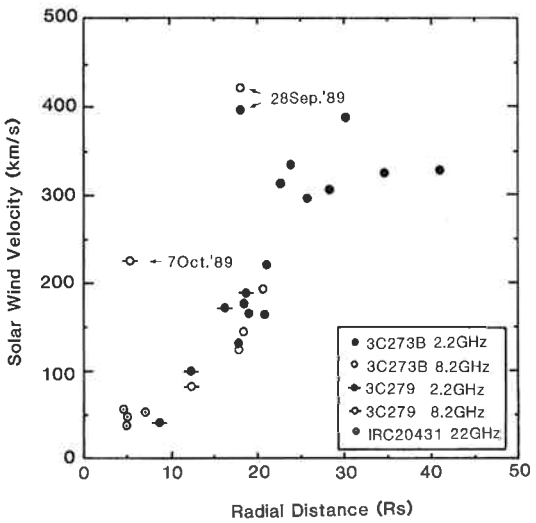

Fig. 7 The radial variation of solar wind velocities derived from Kashima IPS observations in 1989[11]. These results were obtained by the spectral fitting analysis where only the solar wind velocity is assumed to be a free parameter.

correcting this effect.

3.3 Scintillation index measurements

The scintillation index m represents the strength of the scintillation phenomenon, and is defined as follows[34]:

$$m = \frac{\Delta I}{I} \quad \cdots\cdots(12)$$

where ΔI is the magnitude of the radio wave intensity fluctuations, and I is the mean radio wave intensity. The following equation relates m to the IPS power spectrum discussed in section 3.1:

$$m^2 = \frac{\int_0^\infty P(f)df}{I^2} \quad \cdots\cdots(13)$$

When the weak scattering assumption holds, m can be related to the magnitude ΔN_e of solar wind density fluctuations by the following equation[35]:

$$m^2 \propto \lambda^2 \int \Delta N_e^2 dz \sim \lambda^2 (\Delta N_e)^2 L \quad \cdots\cdots(14)$$

where L is the thickness of the layer where radio wave scattering occurs. If we assume the solar wind structure isotropic, we obtain $L \approx R$ and $\Delta N_e \propto R^{-2}$, and thus $m \propto R^{-1.5}$ from Equation (14).

In the Kashima IPS observations, Equation (12) was used to calculate m from the obtained IPS data, and the solar wind density fluctuation distribution was studied using this m data. Since Equation (14) is based on the weak scattering assumption, it is applicable only for the distance range of weak scattering as the spectral fitting method is. In this study, IPS data within the applicable range (i.e.>10 R_S at 2 GHz,>4 R_S at 8 GHz, and>1.7 R_S at 22 GHz) were used for m-index analysis.

4. Results

4.1 Velocity measurement by spectral fitting—Observations in 1989

We derived the solar wind velocity from the Kashima IPS data obtained in 1989, using the spectral fitting method[11]. In this analysis, we optimized our model to the observed spectrum by assuming that the solar wind velocity is a free parameter to be determined. For this optimization we assumed values of $AR=1.5$ and $\alpha=11/3$ (the Kolmogorov value), and we used a suitable value of ΔN_e to fit the observed spectrum. The effects of k_{eq} were ignored here. Figure 7 shows the radial dependence of the solar wind velocity obtained from this analysis. The distance used here (and in the next section) is the distance from the center of the sun to the point P. The figure clearly shows that the solar wind accelerates over the range from 10 R_S to 30 R_S. Since the period of these observations corresponds to a solar maximum, the solar wind structure was considered to be isotropic[37),46]. Therefore, even though these IPS data were taken at different solar latitudes and longitudes, we can safely ignore effects due to latitude and longitude variation. Therefore, it is concluded that the variation of solar wind velocity found in the figure reflects the true solar wind acceleration. Since the final velocity is about 400 km/s, these data are thought to correspond to the acceleration of a slow wind. As shown in the figure, high speed data, which deviate significantly from the averaged curve of the solar wind acceleration, were obtained on two days (September 28 and October 7). These data are interpreted by the passage of unusually fast winds associated with eruption events on the solar surface[36]. From the comparison between this figure and Fig. 1, the Kashima IPS data are found to be less scattered and they provide a acceleration profile more clearly. This is because Fig. 1 was made by combining data taken in different solar activity periods, whereas the observation data shown in Fig. 7 was collected in a relatively short period.

To evaluate the reliability of the solar wind velocity data obtained in this analysis, we compared them with multi-station IPS observations conducted by the Solar-Terrestrial Environment Laboratory (STEL), Nagoya University[37]. The IPS observations made by STEL were used to estimate the solar wind velocity by a cross-correlation method at a frequency of 327 MHz. As result, it is found that five STEL IPS data for 3C273B in 1989 were taken on the same day as the Kashima IPS experiments. A comparison of these simultaneous data shows that $V_3/V_1 = 1.04 \pm 0.29$, where V_3 and V_1 are the solar wind velocities determined at STEL and Kashima respectively. This shows that the velocities obtained by our analysis agree well with STEL velocity data, and that no significant difference exists between them. We also compared the solar wind velocities obtained from the Kashima IPS data taken at 2 GHz and 8 GHz on the same day for the same radio source, and confirmed that they agreed well. (From five pairs of 2 GHz and 8 GHz data, we obtained a ratio of $V_2 / V_8 = 0.94 \pm 0.16$, where V_2 and V_8 are the solar wind velocities determined from the IPS data for 2 GHz and 8 GHz respectively.)

4.2 Multi-Parameter estimation using the spectral fitting method

4.2.1 Observations in 1990

The receiver bandwidth increased in 1990 due to the use of the dedicated back-end, so that the S/N ratio of IPS data was improved greatly. This improvement enabled us to perform the multi-parameter estimation from the Kashima IPS data using the non-linear least-squares method. In the spectral fitting analysis of IPS data obtained in 1990, we included the following parameters as free ones in addition to the solar wind velocity V: the axial ratio AR (anisotropy) of density fluctuations, the power-law index α of the density fluctuation spectrum, the equivalent cut-off frequency k_{eq}, and the magnitude ΔN_e of density fluctuations[12]. Figure 8 shows the radial dependence of the solar wind velocity, axial ratio and spectral index, which were determined from 1990 observations.

Firstly from this figure, the solar wind velocities are found to increase with increasing distance over the range from 10 to 20 R_S. This agrees with the fact that the (low speed) solar wind acceleration was observed in 1989 observations. However, the 1990 velocity data exhibit a larger scatter and the radial profile of the solar wind acceleration is less evident than the 1989 data. Possible reasons for this are as follows:

1. As the effect of fast wind is included in the data for 3C273, the acceleration profile of slow wind may be smeared out by mixing data of different winds.
2. Due to the increase of the axial ratio (described below), the solar wind velocity near the sun may be determined less accurately from the observed power spectrum.
3. Since a large number of variables were taken as free parameters in the spectral fitting analysis, the estimation errors of each parameter may become large.

The axial ratio and spectral index data were found to exhibit systematic variations in the distance range where

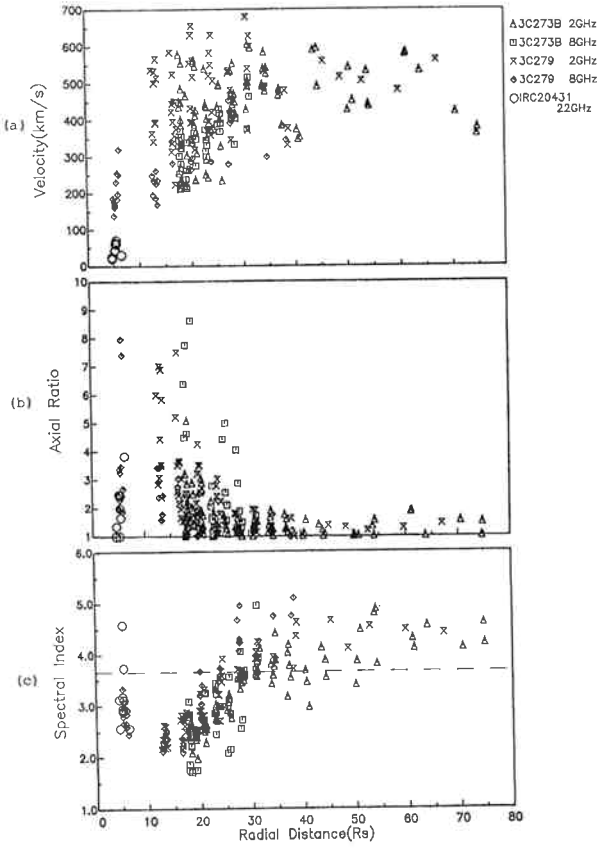

Fig. 8 The radial variations of (a) solar wind velocity, (b) axial ratio, and (c) spectral index obtained from Kashima IPS observations in 1990[12]. The dotted line in (c) indicates the Kolmogorov value ($\alpha = 11/3$).

the solar wind acceleration takes place. The axial ratio data shows that the anisotropy increases with decreasing distance, particularly within the region of 30 R_S. That is, while the axial ratios at larger distances lie about 1-1.15, the axial ratio becomes as high as 2-8 between 5 and 20 R_S. In addition, the axial ratio data are found to display a large scatter near the sun. The spectral index exhibits a value of about $\alpha = 4$, which is slightly higher than the Kolmogorov value ($\alpha = 11/3$), at large distances from the sun, and the spectral index is found to get smaller (i.e. flat spectrum) gradually with decreasing distances up to 30 R_S, reaching $\alpha \approx 2$ around 10 R_S. Furthermore, the spectral index is found to increase with decreasing distance within 10 R_S, and $\alpha \approx 3$ at 5 R_S. As shown in the figure, the variance of the spectral index data is smaller than that of the velocity or axial ratio data.

Earlier studies have shown that the variation of axial ratio increases near the sun[38]. The present study is the first one which demonstrates from systematic observations for a wide distance range that the radial variation of axial ratio is associated those of in solar wind velocity and spectral index, and this fact provides a valuable clue for the study of the physical processes that occur in the solar wind acceleration region. At present,

Coles and Esser[39] propose a model in which the radial variation of axial ratio is explained by an apparent due to Alfvén waves in the solar wind. Recently, the Kashima IPS data has been used to study the variation of axial ratio caused by fast mode and slow mode magnetic wave motion[40], and a fresh discussion has started regarding the mechanism behind the variation of axial ratio with distance. Earlier studies have also shown that the spectral index becomes flat in the vicinity of the sun[41], but the reason for this is still rather unclear. Our observations have demonstrated that the variation of spectral index with distance is synchronized to the variation of solar wind velocity, which suggests that this phenomenon is related to the solar wind acceleration mechanism. Our observations have also resulted in the new finding that the spectral index conversely follows a steep gradient at 5 R_S, which is of great interest in relation to the solar wind acceleration mechanism.

4.2.2 Observations in 1992-1994

Yamauchi et al.[41,42] made a detailed analysis of IPS data obtained for quasars in the period from 1992 to 1994 using the spectral fitting method, and investigated the radial variation of the solar wind velocity, anisotropy, spectral index and inner scale (k_i). The noteworthy point of their analysis were as follows:

1. The IPS data were classified into two groups; i.e. fast wind and slow winds in terms of the solar wind velocity and the position of point P, and the properties of each group were discussed separately.
2. The effect of line-of-sight integration was considered by making the model calculations of the power spectrum with an assumption of a spherically symmetrical structure of the solar wind.
3. The results calculated with a theoretical model of the solar wind acceleration were compared with the results of our IPS observations.

As a result, the following points are clarified:

1. A trend, which suggests the acceleration between 10 and 30 R_S, is observed for slow winds, and this fact agrees with earlier analysis results. The acceleration for fast winds is unclear due to the lack of data near the sun.
2. The spectral index and axial ratio data were found to have a similar radial variation as the results of 1990 observations. No difference was found between fast and slow wind data.
3. For the analysis of the inner scale, a significant difference was found between slow and fast wind data. That is, the inner scale for slow winds was found to deviate greatly from the known radial dependence of the inner scale. When the inner scale is assumed to be associated with the dissipation of magnetohydrodynamic waves[43], the observed deviation is well explained by the effect of the solar wind acceleration between 10 and 30 R_S. On the other hand, the radial variation of inner scale data for fast winds cannot be explained by this effect. A possible reason for this is that density fluctuations in the fast wind are uncorrelated with magnetic filed fluctuations.

4.3 Velocity measurement using the cospectrum method—Observations in 1990-1995

Simultaneous IPS data at 2 GHz and 8 GHz have been available since 1990 from Kashima observations, and this allows us to estimate the solar wind velocity by using the cospectrum method[13]. In Figs. 9 and 10, the solar wind velocities determined by Equation (11) (with $K=1$) from IPS data for 3C279 and 3C273B, respectively, are plotted as a function of the radial distance from the sun. In these figures, velocity data for the period from 1990 through 1995 are shown separately for each year, and in each plot, average values of velocity data over an interval of 2 R_S are indicated. The velocity data for 3C279 (Fig. 9) show that the solar wind velocity gradually increases in the range from 10 to 30 R_S. The terminal velocity is about 400 km/s, so that 3C279 data are thought to represent to the acceleration of a slow wind. A tendency of the solar wind acceleration in the range 10-30 R_S are also seen in velocity data for 3C273B (Fig. 10). These findings agree with the results obtained from the spectral fitting analysis (see the previous section).

Here, we compared the solar wind velocities obtained by the cospectrum method with the velocity data obtained from multi-station IPS observations, as we did in the case of the spectral fitting analysis. Fig. 11 shows the results of the comparison between our data and STEL velocity data taken in 1990-1992. For 1990 and 1992, a good agreement was found between those data, and a value of $V_1/V_3 = 1.04$ ($\sigma_{rms}=0.20$) was obtained. However, a poor correlation was obtained for 1991 data, and a correlation coefficient was just $r=0.7\times10^{-4}$ ($N=18$). While the reason for this is unclear, the fact that difference in estimated velocity for 1991 between Kashima and STEL varies systematically with the radial distance might be a clue to solve this discrepancy. For Kashima velocity data taken in 1993, we made a comparison with IPS solar wind velocity data obtained by EISCAT[45]. Two sets of velocity data were found to correlate very well ($r=0.92$).

The period from 1990 to 1995 corresponds to the maximum and the declining phase of the solar acitivity, and it is clearly found from Figs. 9 and 10 that the solar wind structure changes in association with the variation of the solar activity[14,15,16]. This change is evidently revealed from the velocity peak in the plot of velocity versus distance, and this peak is thought to correspond to a fast wind. The development of fast winds at high latitudes as the solar activity falls was reported from earlier IPS observations[37,46], but there were few studies by which the long-term variation in the solar wind structure near the sun has been clarified from IPS observations. In Kashima IPS observations, the effect of fast wind is seen more prominently in 3C273B data than 3C279 data. That is, the effect of fast wind (i.e. velocity peak) is found in all of 3C273B data except for data taken in 1991, whereas the effect is only observed in 1994 data as for 3C279. This difference is considered to reflect the difference of regions through which the line of sight to these radio sources passed. In Fig. 12, the trajectories of point P in the line of sight to 3C273B and 3C279 for 1993 observations are plotted, being projected on the solar source surface. The

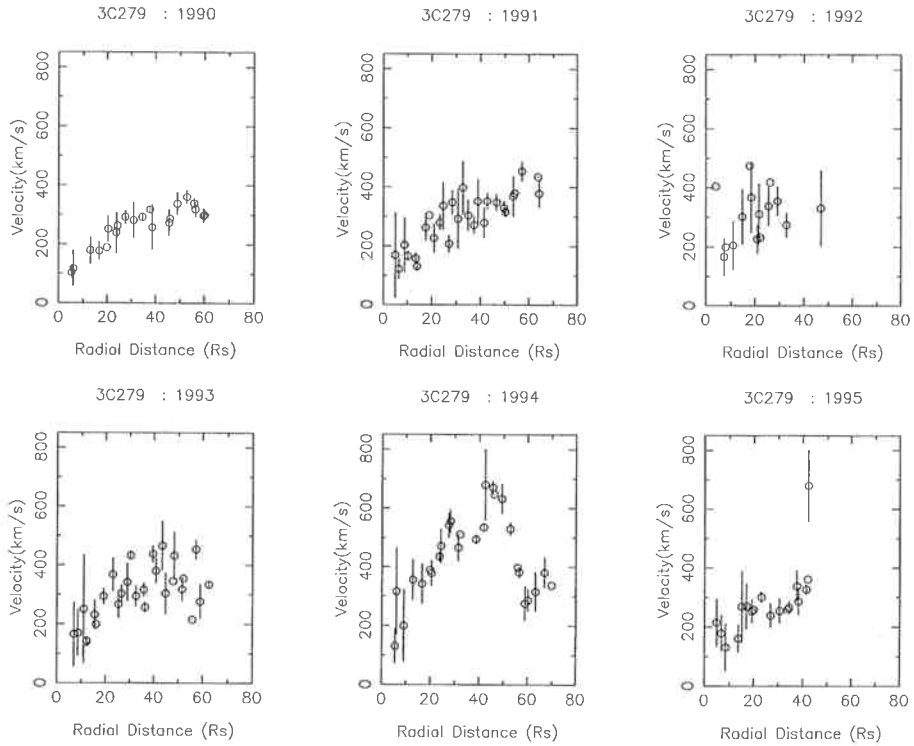

Fig. 9 The radial variation of solar wind velocities obtained from IPS observations for the radio source 3C279 in the period between 1990 and 1995. These velocity measurements were made using the cospectrum method. In this figure, the velocity data for each year are plotted separately, and the data in a given plot are averaged over each interval of 2 R_S. The error bars correspond to a variation of $\pm\sigma$.

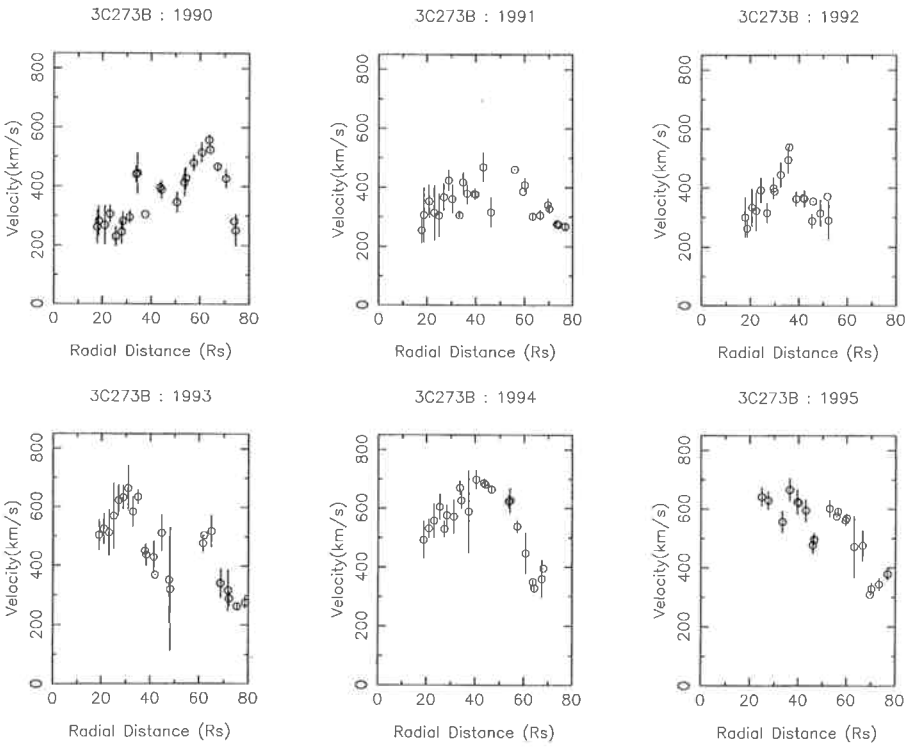

Fig. 10 The radial variation of solar wind velocities obtained from IPS observations for the radio source 3C273B in the period between 1990 and 1995. The format of this figure is the same as in Fig. 9.

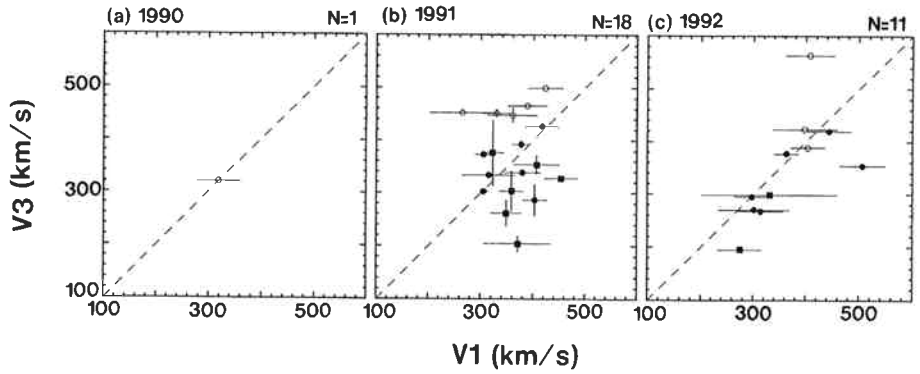

Fig. 11 A comparison of the solar wind velocity V_1 obtained from Kashima IPS observations using the cospectrum method with the solar wind velocity V_3 obtained from multi-station IPS observations by STEL[13]. (a) Results for 1990; (b) results for 1991; (c) results for 1992. The ○ and □ symbols represent data for 3C273B and 3C279 respectively, and the unfilled symbols correspond to data obtained within 30 R_S.

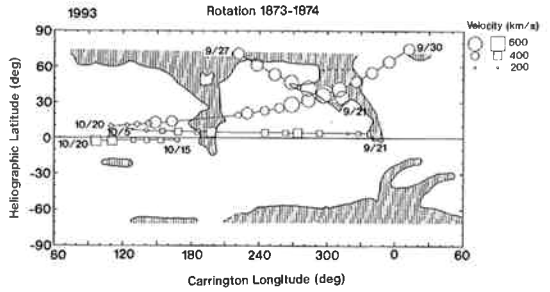

Fig. 12 The trajectories of the point P projected onto the solar source surface for the lines of sight to radio sources 3C273B (○) and 3C279 (□). The size of each symbol represents the solar wind velocity obtained from Kashima IPS observations. The hatched regions correspond to the corona holes from He1803 nm observations (data provided by NOAA/SEC).

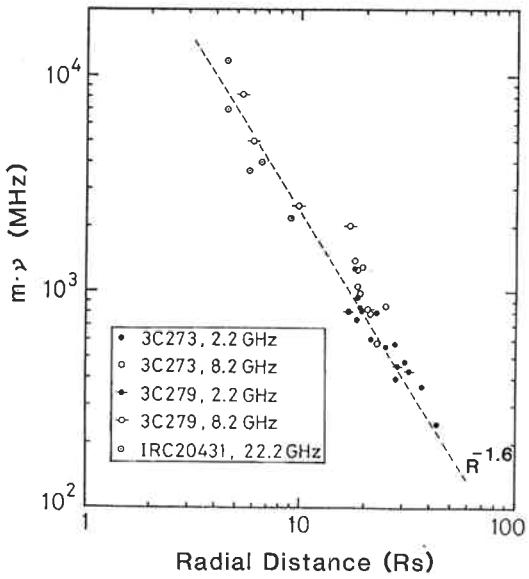

Fig. 13 The radial variation of the scintillation index m obtained from Kashima IPS observations in 1989[11]. To plot m-index data obtained at different frequencies in this figure, the product $m\nu$, where ν is the observation frequency, is taken as a vertical axis.

size of symbols in the figure represents the magnitude of the solar wind speed, and the distribution of the corona hole observed at He1083 nm is also shown in this figure. Corona holes are considered as the source of the fast wind[47], and this figure shows that the solar wind velocity increases as the point P approaches to the corona hole. When the line of sight to 3C273B approaches to the sun, it passes through high latitudes, so that we are more likely to observe the fast wind from the corona hole that develops in the polar region in the quiet period of the solar activity[48]. On the other hand, the line of sight to 3C279 mostly passes through low latitudes and is much less likely to be affected by the corona hole. This effect can explain the difference of the fast wind effect between IPS data for two radio sources.

Since the effect of the fast wind is seen evidently in the Kashima IPS data during periods of the low solar activity, care must be taken when discussing the radial dependence of solar wind velocity from Kashima data. For example, the tendency for solar wind velocity to decrease with distance at large distances from the sun is considered as an apparent effect resulting from the movement of the line of sight from the fast wind to the slow wind. However, it is worth noting that the tendency of the solar wind acceleration, which was observed in both 3C279 and 3C273B data in the range of 10-30 R_S, is hardly explained by the effect of the solar activity change. Although the gradient of the observed velocity increase differs from one year to the next, this is ascribed to the difference of the fast wind. As the solar wind acceleration in the range from 10 to 30 R_S has been clarified from Kashima IPS observations using the different analysis (spectral fitting) method, we confirm here by the cospetrum analysis of Kashima data that the solar wind acceleration takes place certainly in this distance range.

4.4 Distribution of density fluctuations—Observations in 1989-1994

Figure 13 shows the radial variation of the scintillation index determined from Kashima IPS observations in 1989[11]. This figure was produced from m-index data obtained from the two quasars at 2 GHz and 8 GHz, and from the H_2O maser source at 22 GHz. Since the scintillation index m is inversely proportional to the observation frequency ν, the product $m\nu$ is taken as the vertical axis to correct this frequency dependence. The dotted line in this figure shows the curve $R^{-1.6}$ (for $R>0.1$AU) reported by Hewish and Symonds[49], and Kashima IPS data are found to agree well with this curve. Therefore, we conclude that the $R^{-1.6}$ relationship holds to a distance of 5 R_S (0.02 AU) from the sun. The $R^{-1.6}$ relationship is also very close to the curve of $R^{-1.5}$, which is expected for an

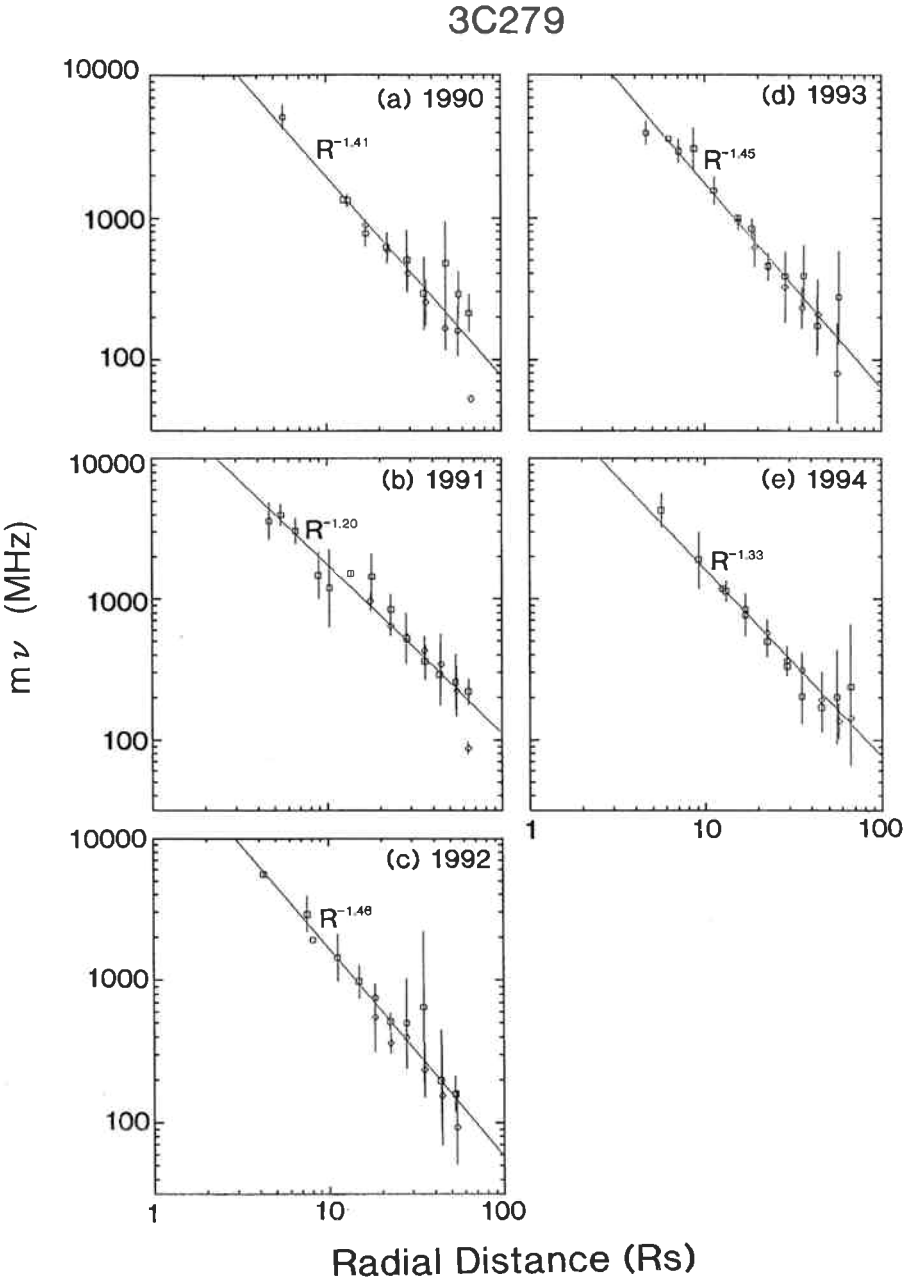

Fig. 14: The radial variation of the scintillation index m obtained from Kashima IPS observations (2 GHz/8 GHz) of 3C279 in the period from 1990 to 1994[15]. As in Fig. 13, the product $m\nu$ is taken as a vertical axis to correct the frequency dependence of m-index. The data is plotted separately on a basis of the observation year, and is averaged over equally-spaced partitions in a logarithmic distance scale for each plot. The error bars correspond to a variation of $\pm\sigma$ from the mean. The dotted line in each plot shows a function aR^{-x} fitted to the observed data.

isotropic distribution of solar wind density fluctuations. Considering that the year of 1989 corresponds to the solar maximum period, we found that this is in good agreement with the fact that the solar wind has an isotropic structure in the solar maximum period[37,46,51]. In the figure, the scintillation index appears to increase slightly in the range 10-30 R_S, which is considered as the acceleration region. This agrees with the properties of the transonic region reported by Lotova et al.[50]. However, we are not currently convinced that this enhancement is significant, because it was not confirmed from the subsequent Kashima IPS observations.

The change of solar wind structure associated with the solar cycle variation, which has been found from Kashima velocity data, is also clearly found from the scintillation index data derived from the Kashima IPS observations[14,15,16]. Figures 14 and 15 show the scintillation index data obtained in the period of 1990-1994 for 3C279 and 3C273B, respectively, being plotted as a function of the radial distance from the sun for each year. The 2 GHz and 8 GHz data are indicated separately in these figures, and the value of $m\nu$ is plotted on the vertical

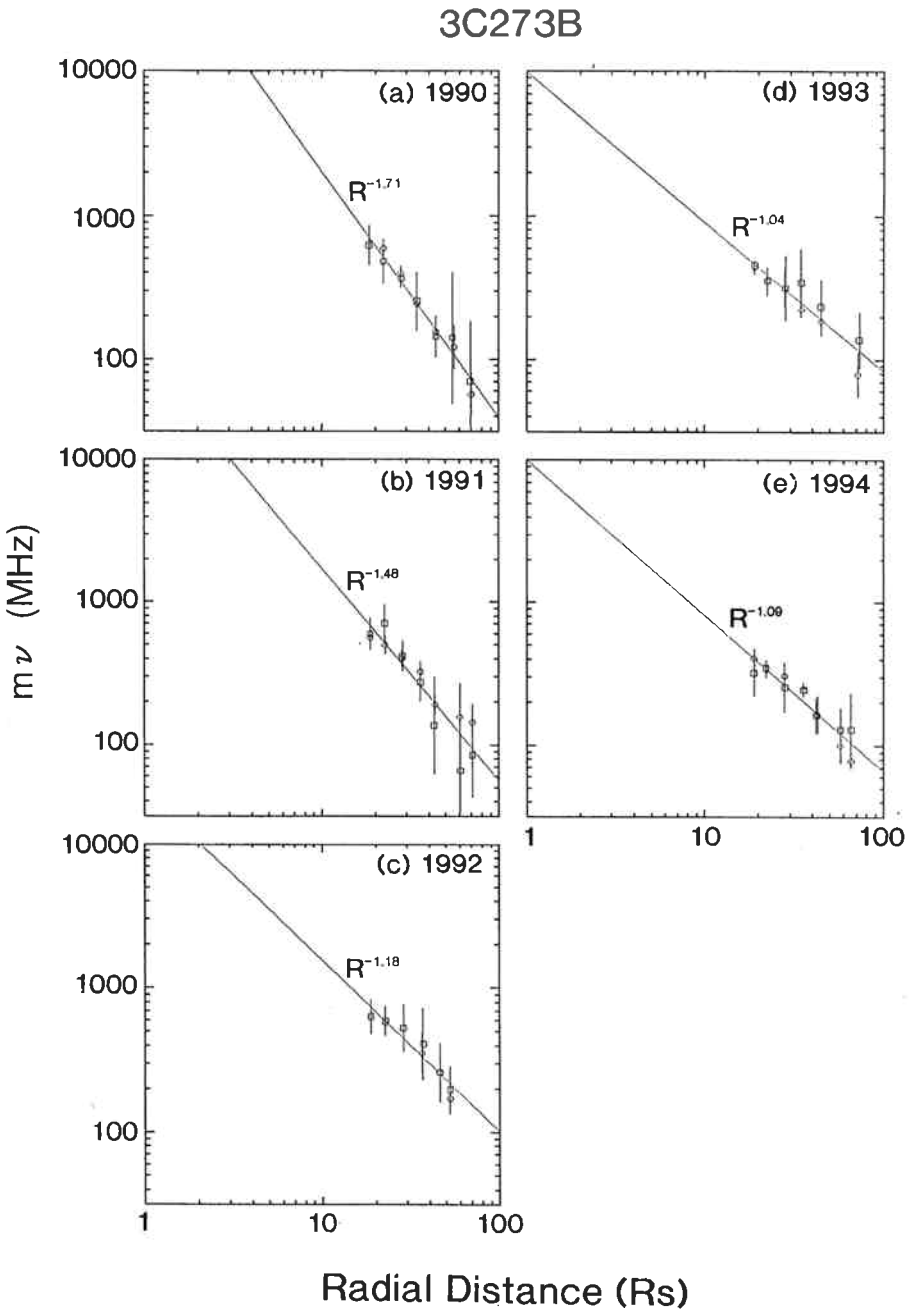

Fig. 15 The radial variation of the scintillation index m obtained from Kashima IPS observations for 3C273B in the period between 1990 and 1994[11]. The format of this figure is the same as in Fig. 14.

axis, as in Figure 13, to correct the frequency dependence of the scintillation index. The dotted lines in the figures correspond to the function $m = aR^{-x}$ fitted to observed data by using the least square method. In 3C279 data (Fig. 14), little change is found in the radial dependence of scintillation index throughout the period analyzed here. However, 3C273B data (Fig. 15) suggest that the radial variation of scintillation index becomes more gradual for this period. Figure 16 shows the radial slope x of the radial variation determined from 3C279 and 3C273B data by the least square method. As this figure shows, the value of x does not vary significantly in 3C279 data in the period of 1990-1994, and it ranges between 1.2 and 1.4. The gradient determined from 3C273B data gradually becomes flatter in this period. The observation result for 3C279 implies that density fluctuations are mostly isotropic in the low latitude region, through which its line of sight passes, and that they are little affected by the solar activity change. On the other hand, the systematic change of the radial slope found for 3C273B data is considered to be due to the development of the corona hole in the polar region in the period of reduced solar activity[48]. That is, the solar wind is more rarified in the corona hole, so that the scintillation index obtained from IPS observations near the sun for 3C273B, whose line of sight passes through high latitude, becomes lower by the effect of the polar corona hole. This explains the long-term change to a flatter radial slope, which was found in 3C273B data. The reduction of density fluctuations in the polar region during the solar minimum also agrees with IPS observations made in Ooty (India)[51].

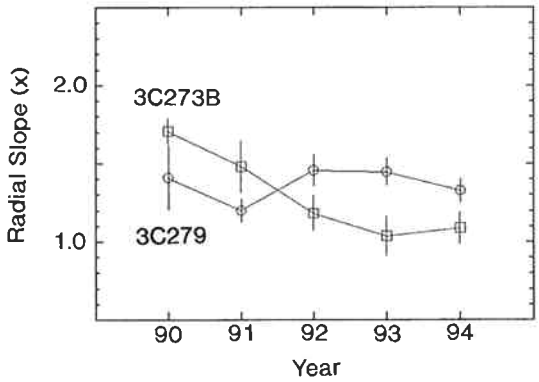

Fig. 16 The annual variation of the radial slope x, determined by fitting the function aR^{-x} to Kashima IPS data by the least square method.

Since the corona holes develop at middle/low latitudes as well as at the polar region, their effects on the scintillation index data can be observed at either a large distance from the sun or near the sun. This is illustrated in Fig. 17, which shows the position of point P for 3C273B and 3C279 projected onto the solar source surface and the corresponding deviation Δm of the scintillation index from the average value. The average value of the scintillation index is determined by fitting the function $m = aR^{-x}$ to the observed data through the least square method. The boundary of the corona hole is indicated in the figure. As shown here, the value of Δm becomes negative when the point P approaches to the corona hole, and the reduction of scintillation index is found to have a one-to-one correspondence with the corona hole.

5. Discussions

5.1 The effect of line-of-sight integration

From Kashima IPS observations, it has been found that the solar wind acceleration for the fast wind as well as the slow wind takes place between 10 and 30 R_S. This

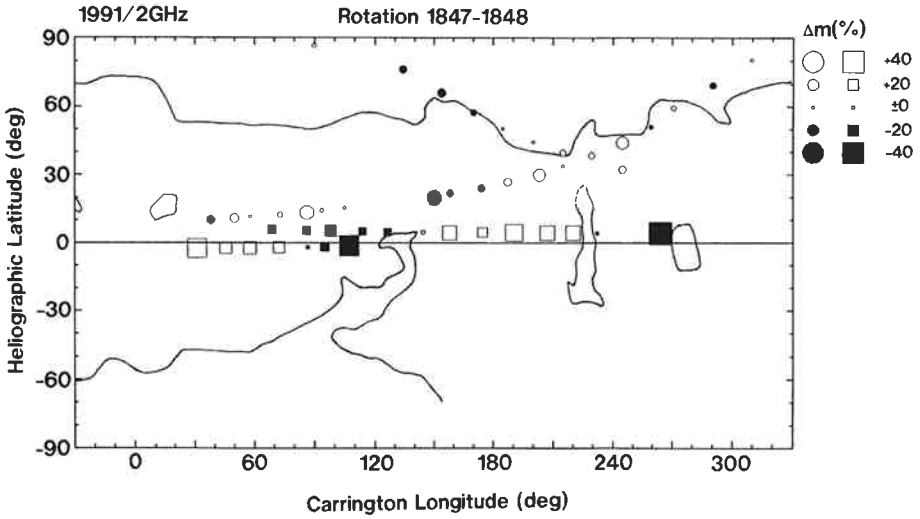

Fig. 17 The trajectories of the point P projected onto the solar source surface for the lines of sight to 3C273B and 3C279 in Kashima IPS observations in 1991. The color (back/white) and size of each symbol represent the deviation Δm from the average value (i.e. the value of a function fitted to the observations) of the scintillation index observed at 2 GHz. The solid lines show the boundary of the corona hole from He1038 nm observations (NOAA/SEC).

result differs considerably from long-baseline IPS observations, which reported that the acceleration of a polar fast wind completes within 10 R_S[25]. This discrepancy might arise from the effect of line-of-sight integration. While the point P approximation was used to analyze Kashima IPS data, this approximation is based on the assumption that the solar wind has an isotropic structure as mentioned earlier (see section 3.1). However, it is demonstrated from out study that the fast wind emanating from the low-density polar region (the corona hole) develops as the solar activity decreases, and this development of the fast wind results in an anisotropic solar wind structure. When the solar wind structure is anisotropic, the results obtained by our analysis may be biased significantly. To estimate the magnitude of any such bias, we performed the calculation of the line-of-sight integration effect using a simple solar wind model[17]. Here, the focus was placed on the velocity increase in the range of 10-30 R_S found from Kashima data for fast winds, and we investigated whether this increase was an intrinsic effect, or an apparent effect resulting from the line-of-sight integration. Accordingly, in our model calculations, we only considered the case where point P in the line of sight passes through a fast wind.

Figure 18 shows the solar wind model used in the model calculations. The solar wind structure in this model is assumed to be symmetrical with respect to the rotation axis, and the solar wind is assumed to consist of three parts: a fast wind at high latitudes (from $\pm 90°$ to $\pm 30°$), a slow wind at low latitudes (from $\pm 20°$ to $0°$) and a medium speed wind between the two. The speeds of the fast and slow winds were assumed to be constant at 700 km/s and 400 km/s respectively, and density fluctuations in the fast wind were assumed to be lower than those in the slow wind by a constant ratio δN_e. Also, the solar wind parameters were assumed to be constant for the fast and slow winds, and were varied for medium speed winds so as to connect between the fast and slow winds linearly.

Using this model, we calculated the integrated cospectrum along the line-of-sight for various solar wind parameters, then we determined the solar wind velocity from the calculated cospectrum using Equation (11) (with K equal to 1.25). Although the solar wind velocities obtained in this way should basically remain constant with varying distance from the sun, they were found to change with distance due to the effect of line-of-sight integration. Figure 19 shows an example of the calculated results. In this figure, the panel (a) shows the results obtained when the ratio of density fluctuations in a fast wind to those in a slow wind was varied with distance, the panel (b) shows the results obtained when the axial ratio of density fluctuations was varied, and the panel (c) shows the results obtained when the spectral index of density fluctuations was varied. It is assumed

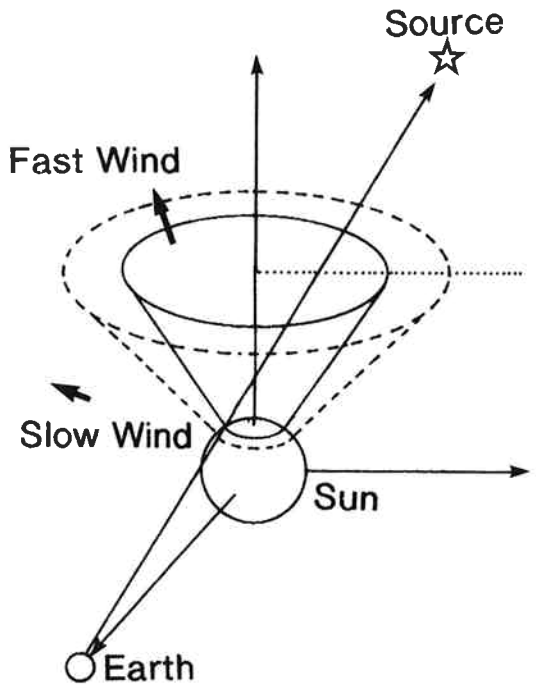

Fig. 18 Schematic illustration of the three-dimensional solar wind model used for our calculations. This model comprises a fast wind (700 km/s) at high latitudes, a slow wind (400 km/s) at low latitudes, and a transition region between the two.

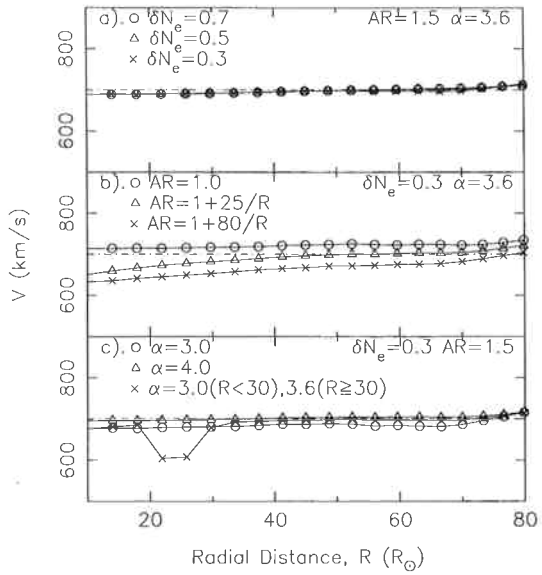

Fig. 19 The radial variation of solar wind velocities obtained from the model calculations of IPS measurements with the cospectrum method[17]. (a) Results obtained when varying the ratio *δNe* of density fluctuations in the fast wind to those in the slow wind. (b) Results obtained when the axial ratio *AR* is allowed to vary with distance. (c) Results obtained when varying the spectral index *α* of density fluctuations.

here that there was no random velocity. This figure shows that the solar wind velocities obtained by the cospectrum method for these three cases (a)-(c) are hardly affected by line-of-sight integration. We also conducted the model calculations in which the solar wind parameters were changed in other ways, and were able to confirm that as long as the effect of random velocity is ignored, the solar wind velocity obtained by the cospectrum method agree with the true velocity with an error less than ±10%.

Table 4 shows the results of model calculations including the effect of the random velocity component δv (parallel to the flow direction). From this table, the velocity obtained by the cospectrum method is found to become larger than the actual velocity, as δv increases. Thus, it is proven that only the random velocity among various solar wind parameters has a significant effect on the measurement of solar wind velocity by the cospectrum method, even when line-of-sight integration is considered. If the acceleration of fast winds between 10 and 30 R_S, which was observed from Kashima IPS data, is an apparent effect caused by the random velocity, this means that the random velocity would be small near the sun, and that it would increase with increasing distance. This is inconsistent with earlier observations in which the random velocity was found to increase near the sun[8], therefore we cannot explain the fast wind acceleration found in Kashima IPS data in terms of the effect of random velocity.

At present, it appears that an explanation for the discrepancy between Kashima observations and long-baseline observations as for the fast wind acceleration may lie in the effect of magnetohydrodynamic (MHD) wave motion near the sun. That is, in IPS observations, the speed at which density fluctuations move through the solar wind is considered to be equal to the bulk flow speed of the solar wind. However, when MHD waves propagate through the solar wind, the propagation velocity of these waves is superimposed on the velocity at which density fluctuations move, and as result the drift speed estimated from IPS observations may not correspond exactly to the actual solar wind velocity. Such an effect by MHD waves may lead to differences between single-station measurements such as Kashima observations and multi-station measurements such as long-baseline observations. Investigations from this viewpoint have just begun and the details on MHD wave effects are not known, and hence it is an important subject for further study.

5.2 Determination of the solar wind acceleration profile using the solar corona data

Since the line of sight passes through both fast winds and slow winds, particularly in periods when the solar activity is low, a careful analysis to separate effects of fast and slow winds is needed in studying the solar wind acceleration profile from IPS observations (see section 3.3). To do this strictly, it would be necessary to make simultaneous observations for several radio sources whose lines of sight cross the solar wind emanating from roughly the same region on the solar surface at different distances from the sun[52]. In addition, the use of computer tomography[33] and/or long-baseline analysis[25,53] methods may be necessary to determine the distribution of fast and slow winds along the line of sight. However, none of these approaches can be applied to Kashima IPS observations, which were made at a single station using a very limited number of radio sources.

In the present study, therefore, the acceleration profile has been studied by dividing Kashima data into fast, intermediate and slow winds according to data of the solar corona brightness intensity at the location of the line of sight point P projected onto the solar source surface, and then the radial variation of the speed has been determined for each wind[17]. This analysis method is based on the fact—established by earlier observations—that dark and bright regions in the solar corona respectively correspond to regions from which fast winds (corona holes) and slow winds emanate[46,54]. As shown by the model calculations in the previous section, the solar wind velocities obtained by the cospectrum method are little affected by line-of-sight integration, and they closely agree with the velocity at point P. So that, it should be possible to treat fast and slow winds separately by classifying the velocity data according to the corona brightness intensity at the point P projected on the solar source surface. As for the solar corona brightness data, we used the K corona data obtained with the Mk III coronagraph at the Mauna Loa solar observatory in Hawaii (at an altitude of 1.36 R_S from the sun). When determining velocities with the cospectrum method, we used $K=1.25$ and we assumed the solar wind to flow at a uniform velocity in the radial direction, when the point P is projected onto the solar source surface.

Figure 20 shows the relationship between the solar

Table 4 The errors caused by the random velocity δv parallel to the flow in solar wind velocity measurements through the cospectrum method (with $K=1.25$). While the velocities estimated by the cospectrum method should match the fast wind speed of 700 km/s, the effect of the random velocity biases the estimated velocity to a higher value.

δv	V_{ZERO} at $10\,R_S$	V_{ZERO} at $70\,R_S$
70 km/s	717 km/s	730 km/s
210 km/s	818 km/s	832 km/s
350 km/s	1014 km/s	1032 km/s
560 km/s	1368 km/s	1395 km/s

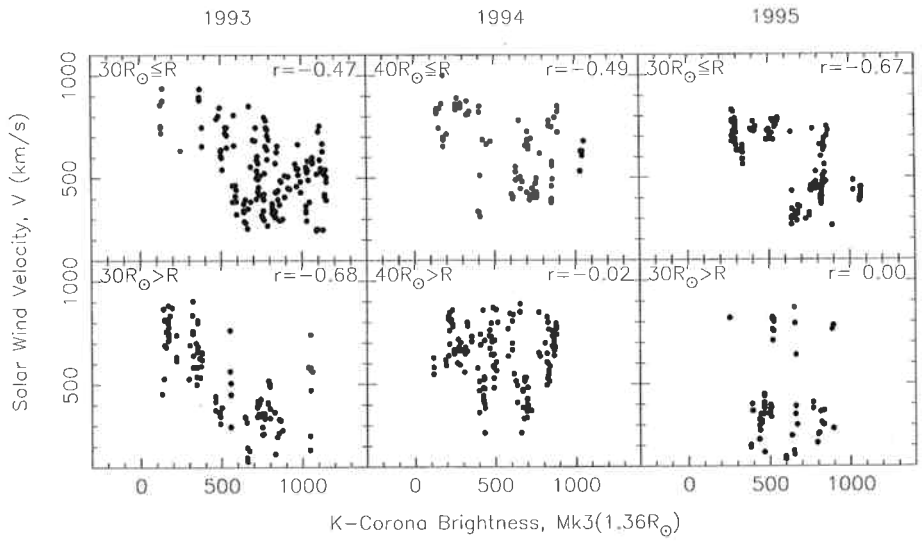

Fig. 20 The relation between the corona brightness intensity and the solar wind speed at the point P projected onto the solar source surface[17]. The data is grouped on a basis of the observation year, and the upper and lower panels for a given year correspond to the data for $\geq 30\ R_S$ and $\geq 30\ R_S$ respectively.

wind velocities determined from Kashima IPS data taken in 1993-1995 (using the cospectrum method) and the K corona brightness intensity at the projected position of point P. In this figure, data are divided into two sets; those lying in the distance range where the solar wind acceleration was observed, and those lying outside this distance range (>30 or >40 R_S). Outside the acceleration region, an inverse correlation is found from this figure between the solar wind velocity and the K corona brightness intensity, and this fact is in agreement with earlier observations[46,54]. The correlation between the speed and corona brightness is unclear in the acceleration region, and this is probably due to the effect of solar wind acceleration (although an inverse correlation is found in the acceleration region for 1993 data). This inverse correlation between the solar wind velocity and the K corona brightness intensity in the radial range where the solar wind acceleration completes suggests that we can use the K corona brightness to separate fast and slow winds.

Figure 21 shows the radial variation of solar wind velocity determined by classifying Kashima IPS data into three groups corresponding to bright, intermediate and dark K corona intensity at the position of point P projected onto the solar source surface (2.36 R_S). The bright, intermediate and dark regions of the K corona intensity are expected to correspond to slow, intermediate and fast winds, respectively. As the figure shows, the terminal solar wind velocities for bright and dark corona data correspond to about 400 km/s and 700-800 km/s, respectively, which match with velocities of slow and fast winds. Regions of intermediate K corona brightness were found to correspond to solar winds having intermediate terminal velocities lying between those of fast and slow winds. Thus, the K corona brightness intensity appears to act as a useful guide for separating the data into fast and slow winds.

As for the radial variation of the solar wind velocity, which is the most important in this analysis, the figure suggests that the acceleration continues up to 20 R_S for slow, intermediate and fast winds. This confirms the conclusion obtained by our IPS studies, which demonstrate that the solar wind acceleration occurs at 10-30 R_S. The data for the intermediate-speed wind show that the speed decreases with increasing distance at large distances. This variation is not considered as an intrinsic one, and it is probably due to incomplete separation of slow and fast winds, resulting in a mixture between radial variations for both types of wind.

5.3 The effects of magnetohydrodynamic wave motion

In section 3.2.2 we mentioned that the anisotropy of solar wind density fluctuations inferred from IPS observations may be affected by magnetohydrodynamic (MHD) wave motion. Also, in section 4.1 we stated that the velocity obtained from multi-station IPS observations could be affected by MHD wave motion. MHD wave motion is thought to play an important role in the solar wind acceleration and the corona heating[4]. If this effect is extracted through the IPS observations, it will provide important clues for studying the mechanisms of solar wind acceleration and corona heating. Attempts to analyze IPS observations from a viewpoint of studying MHD wave motion have just begun, and analysis procedures have never established yet. Here, we would like to report one of such attempts, which is based on the cospectrum analysis employed for Kashima IPS observations[55].

Figure 22 shows an example of the calculated cospectrum calculation for the case where the slow-mode MHD wave motion is present. As this figure shows, a fluctuation in the correlation, which swings in the negative direction, appears at lower frequencies. Some parameters, which characterize MHD wave motion in the solar wind, may be inferred from the shape of this

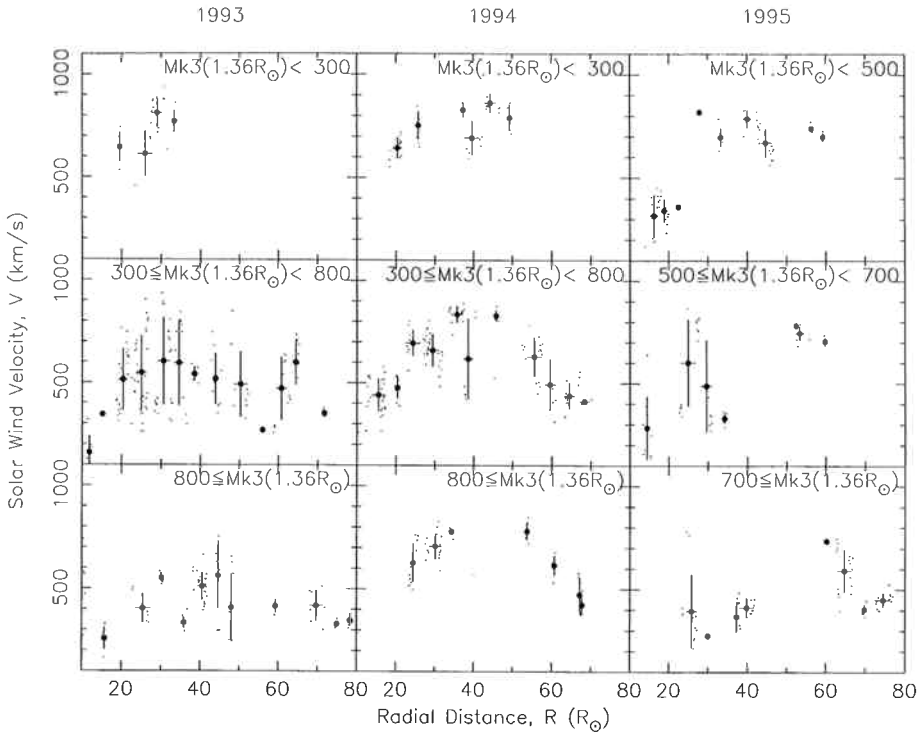

Fig. 21 The radial dependence of solar wind velocities obtained by sorting Kashima IPS data into a bright region (lower panel), an intermediate region (middle panel) and a dark region (upper panel), based on the corona brightness intensity data at the point P projected onto the solar source surface[17]. Large black circles in each plot show the average values over an distance interval with 5 R_S width, and the error bars correspond to a variation of $\pm\sigma$.

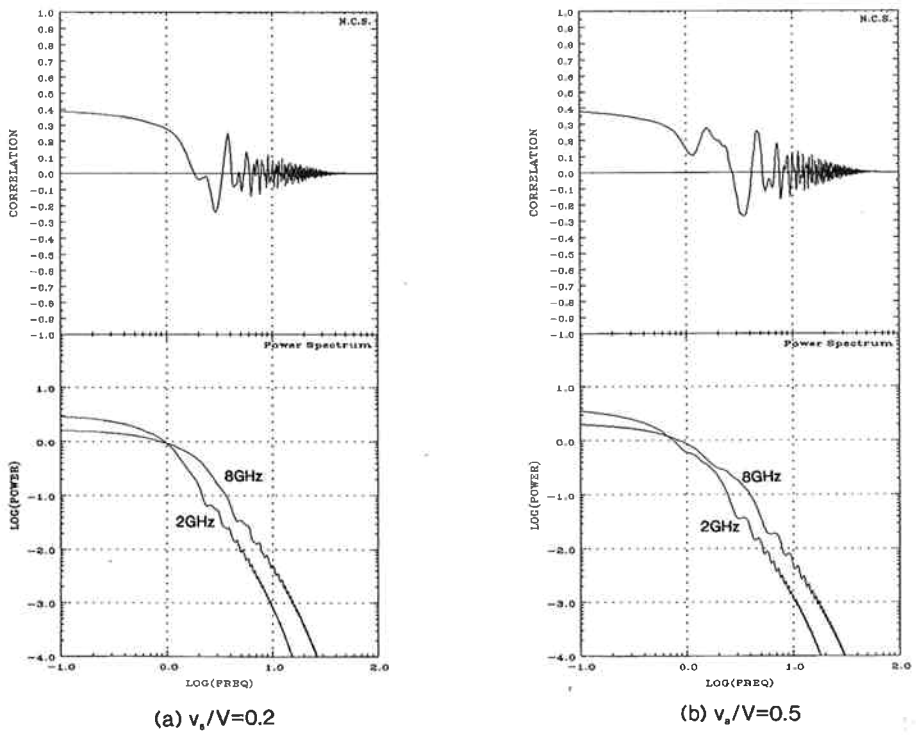

Fig. 22 Model calculations of the power spectrum (bottom) and cospectrum (top), when the effect by the slow mode MHD wave is considered[55]. The ratio of the MHD wave propagation velocity to the solar wind velocity is assumed to be (a) $v_s/V=0.2$, and (b) $v_s/V=0.5$.

fluctuation and the corresponding frequencies. In fact, cospectra resembling this figure were found in Kashima IPS data. We expect that further analysis of IPS data will shed more light on the MHD wave motion in the vicinity of the sun.

6. Conclusions

From 1989 to 1998, IPS observations were made using three microwave frequencies (2 GHz. 8 GHz and 22 GHz) at the Kashima Space Research Center, and obtained IPS data have been used to study the solar wind acceleration mechanism, which is not fully understood yet. As a result, we have clarified the following points:

1. We have used spectral fitting and cospectrum methods to derive the solar wind velocity near the sun from Kashima IPS observations. From the analysis of the radial variation of obtained velocity data, it became clear that acceleration of the slow solar wind takes place in the distance range of 10-30 R_S from the sun. It should be noted here that a similar trend was also found for fast winds, and this fact differs significantly from recent observation, which show that the acceleration of fast winds finishes within 10 R_S from the sun[25]. We have shown that this discrepancy cannot be explained by either the effect of line-of-sight integration or the effect of line-of-sight movement in the latitude/longitude. One possibility to reconcile the discrepancy is that IPS observations are affected by MHD wave motion, although the detailed discussion is deferred to a further study.
2. Using the spectral fitting method, we have investigated the spatial spectrum of density fluctuations close to the sun from Kashima IPS data. As a result, we have found that the anisotropy increases near the sun and the spectral gradient becomes more gradual than the Kolmogorov value ($\alpha = 11/3$) there. The region in which these effects occur matches the acceleration region, so that it is inferred that these phenomena are associated with the acceleration mechanism. However, the details of this mechanism are still unclear. We has discovered from Kashima IPS data that the inner scale of the density fluctuation spectrum departs significantly from the radial variation, which was reported from the earlier IPS study, in the solar wind acceleration region. We have shown that then the observed variation of the inner scale can be well explained by an acceleration model for the case of slow winds under assumption where this departure is associated with the dissipation of Alfven waves. However, no explanation is found for fast winds, and further study is needed.
3. By analyzing the scintillation index, we have shown that the distribution of density fluctuations in the solar maximum is well expressed by a radial variation of $R^{-1.6}$ down to regions very close to the sun (≈ 5 R_S)
4. From the subsequent long-term Kashima IPS observations, we have obtained a clear picture of the solar cycle change in the solar wind structure near the sun. That is, during the solar maximum, the distribution of density fluctuations is isotropic and the solar wind is dominated by slow winds. However, when the solar activity decreases, the corona hole (which is a source of the fast wind) develops in the sun's polar region and density fluctuations in the polar region become lower than those at the equator. We have shown from Kashima IPS data that the solar wind structure at low latitudes changes little with variations of solar activity, and that the slow wind predominates around the equator throughout the solar cycle. We have also shown that the location of the solar wind acceleration region is mostly unchanged throughout the solar cycle.
5. From Kashima IPS observations, we are unable to confirm the significant enhancement of density fluctuations in the solar wind acceleration region.

Based on these results of Kashima IPS observations, we plan to conduct two-station microwave IPS observations in the near future in order to shed more light on solar wind acceleration. In this plan, two large antennas—the 34 m antenna at Kashima and the 64 m antenna at Usuda Deep Space Center (the Institute of Space and Astronautical Science)—are used to perform IPS observations for the 8 GHz beacon signal from the Mars Orbitor *Nozomi*, around its solar conjunction, which is expected to occur from late 2000 to early 2001[56]. The long-baseline analysis technique will be employed to analyze the *Nozomi* IPS observations. This technique was developed by the group at UCSD, and is well known as the technique used to clarify the rapid acceleration of a polar fast wind[25]. Their result of the rapid acceleration has never examined by independent research groups yet, so that further study to confirm is required. The *Nozomi* IPS observations will provide a chance to verify the rapid accelaration, and also provide the key to resolving the discrepancies between Kashima IPS observations and long-baseline IPS observations.

The region, which is though to be important for clarifying the acceleration of solar wind, has shifted closer to the sun over the last 10 years. Consequently, IPS observations of H_2O maser sources at 22 GHz, which allow us to probe the solar wind as close as 5 R_S, has become of greater importance ever before. Unfortunately, IPS data for the H_2O maser source has been unavailable since 1995 from Kashima observations. Nevertheless, VLBI solar wind observations at 22 GHz were made in the period between the end of 1997 and early 1998 using the JNET. Although these VLBI experiments were beset with various difficulties such as bad weather and critical defects, we still managed to obtain successfully some valuable data. Those data is now used to analyze the spectrum of plasma density turbulence near the sun[57]. We expect that we will have more opportunities to perform high frequency IPS observations and VLBI solar wind observations in the future.

Acknowledgments

We are indebted to Dr. Hirotaka Mori (the Space Science Division of CRL at that time) for getting this study started. We would also like to thank all staffs of

the Radio Astronomy Applications Group of CRL for their assistance in making Kashima IPS observations. We gratefully acknowledge Dr. Takashi Tanaka (the Space Sciences Division of CRL) and other staffs of CRL, Professor Masayoshi Kojima of the Solar-Terrestrial Environment Laboratory (STEL), Nagoya University, and other members of the solar wind group for their help. We are grateful to staffs at the Geographical Survey Institute for allowing us to use their 26 m antenna when the Kashima 34 m antenna was out of use.

References

(1) Parker, E.N., "Dynamics of the interplanetary gas and magnetic fields", Astrophys. J., 128, pp.664-676, 1958.

(2) Neugebauer, M., and C.W. Snyder, "Mariner 2 observations of the solar wind, 1: Average properties", J. Geophys. Res., 71, pp.4496-4484, 1966.

(3) Marubashi, K., "Space weather forecast program", Space Sci. Rev., 51, pp.197-214, 1989.

(4) Barnes, A., "Acceleration of the solar wind", Rev. Geophys., 30, pp.43-55, 1992.

(5) Bird, M.K. and P. Edenhofer, "Remote sensing observations of the solar corona", in "Physics of the inner heliosphere, 1: Large-scale phenomena", edited by R. Schwenn and E. Marsch, Springer-Verlag, pp.13-97, 1990.

(6) Bourgois, G., Interplanetary scintillation of radiosources at 2695 MHz, Astron. Astrophys., 2, pp.209-217, 1969.

(7) Ekers, R.D., and L.T. Little, "The motion of the solar wind close to the sun", Astron. Astrophys., 10, pp.310-316, 1971.

(8) Armstrong, J.W., and R. Woo, "Solar wind motion within 30 $R_\odot$: Spacecraft radio scintillation observations", Astron. Astrophys., 103, pp.415-421, 1981.

(9) Hewish, A., P.F. Scott, and D. Wills, "Interplanetary scintillation of small diameter radio sources", Nature, 203, pp.1214-1217, 1964.

(10) Coles, W.A., "Interplanetary scintillation", Space Sci. Rev., 21, pp.411-425, 1978.

(11) Tokumaru, M., H. Mori, T. Tanaka, T. Kondo, H. Takaba, and Y. Koyama, "Solar wind near the sun observed with interplanetary scintillation using three microwave frequencies", J. Geomag. Geoelectr., 43, pp.619-630, 1991.

(12) Tokumaru, M., H. Mori, T. Tanaka, T. Kondo, H. Takaba, and Y. Koyama, "Observations of solar wind near the sun from microwave IPS phenomena", COSPAR Colloquia Series Vol.3, Solar Wind Seven, pp.289-292, 1992.

(13) Tokumaru, M., T. Kondo, H. Mori, and T. Tanaka, "Solar wind motion near the sun derived from simultaneous interplanetary scintillation observations at 2 GHz and 8 GHz", J. Geomag. Geoelectr., 46, pp.835-849, 1994.

(14) Tokumaru, M., H. Mori, T. Tanaka, T. Kondo, "Evolution of the solar wind structure in the acceleration region during 1990-1993 (STEP Interval)", J. Geomag. Geoelectr., 47, pp.1113-1120, 1995.

(15) Tokumaru, M., T. Kondo, H. Takaba, H. Mori, and T. Tanaka, "Evolution of the solar wind acceleration region during 1990-1994", Proc. International Solar Wind Eight Conference (AIP Conference Proc. No.382), pp.121-124, 1995.

(16) Tokumaru, M., H. Mori, T. Tanaka, T. Kondo, and H. Takaba, "Observations of the solar wind close to the sun by interplanetary scintillation", Proc. STPW '96, pp.138-141, 1997.

(17) Tokumaru, M., M. Kojima, T. Ohmi, T. Kondo, and K. Hakamada, "Radial variation of solar wind velocity near the sun", Proc. Solar Wind 9, pp.313-316, 1999.

(18) Tokumaru, M., H. Mori, T. Tanaka, T. Kondo, H. Takaba and Y. Koyama, "Studies of solar wind and solar wind-magnetosphere interaction from the ground-based observations of natural radio sources", Proceedings of the first STEP symposium, pp.148-156, 1990.

(19) Mori, H., T. Tanaka, T. Kondo, M. Tokumaru, H. Takaba and Y. Koyama, "IPS observation of the solar Wind acceleration region at microwave frequencies", Proceedings of the second STEP symposium, pp.121-128, 1991.

(20) Tokumaru, M., H. Mori, T. Tanaka, T. Kondo, H. Takaba and Y. Koyama, "Studies on solar wind acceleration region by interplanetary scintillation measurements at microwave frequencies", Proceedings of the third STEP symposium, pp.97-105, 1992.

(21) Tokumaru, M., H. Mori, T. Tanaka, T. Kondo, H. Takaba and Y. Koyama, "A study of the near-sun solar wind by interplanetary scintillation measurements using microwave frequencies (II)", Proceedings of the fourth STEP symposium, pp.212-220, 1993.

(22) Tokumaru, M., H. Mori, T. Tanaka, and T. Kondo, "Distribution of turbulence and mass flux density in the acceleration region of the solar wind", Proceedings of the Eighth International Symposium on Solar Terrestrial Physics, p.21, 1994.

(23) Tokumaru, M., H. Mori, T. Tanaka, T. Kondo, and H. Takaba, "Study of the near-sun solar wind by interplanetary scintillation measurements using microwave frequencies (III)", Proceedings of the sixth STEP symposium, pp.238-247, 1995.

(24) Philips, J.L, A. Balogh, S.J. Bame, B.E. Goldstein, J.T. Gosling, J.T. Hoeksema, D.J. McComas, M. Neugebauer, N.R. Sheeley, Jr., and Y.-M. Wang, "ULYSSES at 50° south: Constant immersion in the high-speed solar wind", Geophys. Res. Lett., 21, pp.1105-1108, 1994.

(25) Grall, R.A., W.A. Coles, M.T. Klinglesmith, A.R. Breen, P.J.S. Williams, J. Markkanen, and R. Esser, "Rapid acceleration of the polar solar wind", Nature, 379, pp.429-432, 1996.

(26) Koyama, Y., H. Takaba, N. Kurihara, and N. Kawaguchi, "The 34 m antenna system of Kashima station", Rev. CRL (Special Issue). **36**. 8, pp.39-50, Jan. 1990.

(27) Dennison, P.A., and A. Hewish, "The solar wind outside the plane of the ecliptic", Nature, 213, pp.343-346,

1967.
(28) Coles, W.A., and J.K. Kaufman, "Solar wind velocity estimation from multi-station IPS", Radio Sci., 13, pp.591-597, 1978.
(29) Manoharan, P.K., and S. Ananthakrishnan, "Determination of solar-wind velocities using single-station measurements of interplanetary scintillation", Mon. Not. Roy. Astron. Soc., 244, pp.691-695, 1990.
(30) Scott, S.L., B.J. Rickett, and J.W. Armstrong, "The velocity and density spectrum of the solar wind from simultaneous three-frequency IPS observations", Astron. Astrophys., 123, pp.191-206, 1983.
(31) Scott, S.L., W.A. Coles, and G. Bourgois, "Solar wind observations near the sun using interplanetary scintillation", Astron. Astrophys., 123, pp.207-215, 1983.
(32) Cronyn, W.M., "Density fluctuations in the interplanetary plasma: Agreement between space-probe and radio scattering observations", Astrophys. J., 171, pp.L101-L105, 1972.
(33) Kojima, M., M. Tokumaru, H. Watanabe, A. Yokobe, K. Asai, B.V. Jackson, and P.L. Hick; "Heliospheric tomography using interplanetary scintillation observations, II: Latitude and heliocentric distance dependence of solar wind structure at 0.1-1 AU", J. Geophys. Res., 103, pp.1981-1989, 1998.
(34) Cohen, M.H., E.J. Gundermann, H.E. Hardebeck, and L.E. Sharp, "Interplanetary scintillations, II: Observations", Astrophys. J., 147, pp.449-466, 1967.
(35) Salpeter, E.E., "Interplanetary scintillations, I: Theory", Astrophys. J., 147, pp.433-448, 1967.
(36) Woo, R., and J.W. Armstrong, "Measurements of a solar flare-generated shock wave at 13.1 R_0", Nature, 292, pp.608-610, 1981.
(37) Kojima, M., and T. Kakinuma, "Solar cycle dependence of global distribution of solar wind speed", Space Sci. Rev., 53, pp.173-222, 1990.
(38) Armstrong, J.W., W.A. Coles, M. Kojima, and B.J. Rickett, "Observations of field-aligned density fluctuations in the inner solar wind", Astrophys. J., 358, pp.685-692, 1990.
(39) Coles, W.A., and R. Esser, "An observational limit to the amplitude of Alfven waves in the solar wind and comparison with an acceleration model", J. Geophys. Res., 97, pp.19139-19148, 1992.
(40) Chashei, I.V., M. Kojima, and M. Tokumaru, "Anisotropy of magnetosonic turbulence in the solar wind between 0.1 and 0.4 AU", J. Geophys. Res., in press, 2000.
(41) Woo, R., and J.W. Armstrong, "Spacecraft radio scattering observations of the power spectrum of electron density fluctuations in the solar wind", J. Geophys. Res., 84, pp.7288-7296, 1979.
(42) Yamauchi, Y., M. Kojima, M. Tokumaru, H. Misawa, H. Mori, T. Tanaka, H. Takaba, T. Kondo, and P.K. Manoharan, "Micro-turbulence in the solar wind at 5-76 R_S observed with interplanetary scintillation", J. Geomag. Geoelectr., Vol. 48, pp.1201-1217, 1996.
(43) Yamauchi, Y., M. Tokumaru, M. Kojima, P.K. Manoharan, R. Esser, "A study of density fluctuations in the solar wind acceleration region", J. Geophys. Res., Vol. 103, pp.6571-6583, 1998.
(44) Coles, W.A., and J.K. Harmon, "Propagation observations of the solar wind near the sun", Astrophys. J., 337, pp.1023-1034, 1989.
(45) Bourgois, G., W.A. Coles, G. Daigne, J. Silen, T. Turunen, and P.J. Williams, "Measurements of the solar wind velocity with EISCAT", Astron. Astrophys., 144, pp.452-462, 1985.
(46) Rickett, B.J., and W.A. Coles, "Evolution of the solar wind structure over a solar cycle: Interplanetary scintillation measurements compared with coronal observations", J. Geophys. Res., 96, pp.1717-1736, 1991.
(47) Krieger, A.S., A.F. Timothy, and E.C. Roelof, "A coronal hole and its identification as the source of a high velocity solar wind stream", Sol. Phys., 29, pp.505-525, 1973.
(48) Hundhausen, A.J., R.T. Hansen, and S.F. Hansen, "Coronal evolution during the sunspot cycle: Coronal hole observed with the Mauna Loa K-coronameters", J. Geophys. Res., 86, pp.2076-2094, 1981.
(49) Hewish, A., and M.D. Symonds, "Radio investigation of the solar plasma", Planet. Space Sci., 17, pp.313-320, 1969.
(50) Lotova, N.A., D.F. Blums, and K.V. Vladimirskii, "Interplanetary scintillation and the structure of the solar wind transonic region", Astron. Astrophys., 150, pp.266-272, 1985.
(51) Manoharan, P.K., "Three-dimensional structure of the solar wind: Variation of density with the solar cycle", Sol. Phys., 148, pp.153-167, 1993.
(52) Coles, W.A., R. Esser, U.-P. Lφvhaug, J. Markkanen, "Comparison of solar wind velocity measurements with a theoretical acceleration model", J. Geophys. Res., 96, pp.13849-13859, 1991.
(53) Breen, A.R., W.A. Coles, R.R. Grall, M.T. Klingsmith, J. Markkanen, P.J. Moran, B. Tegid, P.J.S. Williams, "EISCAT measurements of the solar wind", Ann. Geophys., 14, pp.1235-1245, 1996.
(54) Sime, D.G., and B.J. Rickett, "Coronal density and the solar wind speed at all latitudes", J. Geophys. Res., 86, pp.8869-8876, 1981.
(55) Shishov, V.I., and M. Tokumaru, "Temporal spectrum of interplanetary scintillation in the near-Sun region", J. Geomag. Geoelectr., Vol.48, pp.1461-1480, 1996.
(56) Tokumaru, M., M. Kojima, K. Fujiki, A. Yokobe, K. Oyama, and T. Kondo, "Observation of the solar wind using a Mars probe beacon signal", Proc. 1999 magnetosphere/ionosphere symposium, pp.58-61, 1999.
(57) Shimizu, Y., M. Tokumaru, M. Kojima, "VLBI observation of solar wind plasma", Proc. 1998 VLBI symposium, pp.35-38, 1998.